The Design of an Imidazolium Functionalized SIFSIX Pillared Metal-Organic Framework

By

Daniel John O'Hearn

A Thesis Submitted to

Saint Mary's University, Halifax, Nova Scotia

in Partial Fulfillment of the Requirements for

the Degree of Bachelor of Science

with Honours in Chemistry.

April, 2017, Halifax, Nova Scotia

Certification

The Design of an Imidazolium Functionalized SIFSIX Pillared Metal-Organic Framework

I hereby certify that this thesis was carried out by Daniel John O'Hearn in partial fulfillment for the requirements of the Degree of Bachelor of Science, Honours in Chemistry at Saint Mary's University. I certify that this is truly original work carried out by Daniel John O'Hearn.

Reader:

Dr. Jason D. Masuda

_____

Date: April 24, 2017

Supervisor and Chairperson of the Chemistry Department:

Dr. Robert D. Singer

_____

Date: April 24, 2017

Abstract

The Design of an Imidazolium Functionalized SIFSIX Pillared Metal-Organic Framework

By: Daniel John O'Hearn

Metal-organic frameworks have become a popular research topic for the design of functional materials. Their high surface area and regular pore size combined with their tunability have resulted in applications in gas adsorption, separations, and catalysis. These properties can be improved by functionalization of the internal scaffolding, resulting in materials that are highly task specific. When the SiF_6^{2-} anion is used as a pillar in the design of a metal-organic framework, the resulting material has demonstrated extremely selective uptake of both carbon dioxide[1] and acetylene[2] from gas mixtures. Since imidazolium salts have been shown trap carbon dioxide by chemisorption,[3] it is hypothesized that an imidazolium functionalized SiF_6^{2-} pillared metal-organic framework would possess an enhanced ability to capture carbon dioxide. In this work, the design strategy, and synthesis of an imidazolium functionalized SiF_6^{2-} pillared, metal-organic framework is discussed.

1. Nugent, P. *et al. Nature*. **2013**, *495*, 80-85.
2. Cui1, X. *et al. Science*. **2016**, *353(6295)* 141-144.
3. Mao, J. X. *et al. Phys. Chem. Chem. Phys*. **2016**, *18*, 1911-1917.

Acknowledgements

I would like to start by thanking my supervisor, Dr. Robert Singer for mentoring me and providing me with the opportunity to work in his research lab. Not only did he provide me with guidance in my research, but he also provided me with an environment to learn through experience, which has been an invaluable opportunity for me. I would also like to thank Dr. Bitu Hurriso, and J. Kyle Awalt for teaching me the ins and outs of working in the lab. A heartfelt thank also goes out to the rest of the Singer Group for their support and companionship over this past year.

I would also like to thank Dr. Kathy Robertson, Dr. Jason Masuda, Alex Vienot, and Darcie Stack for teaching me how to use the X-ray diffractometer and for their guidance in structure refinement. Alyssa Doué, Darlene Goucher, and Elizabeth McLeod for their technical support, and for ensuring that the chemistry department runs smoothly, and Dr. Patricia Granados for providing mass spectrometry analysis.

I would like to thank my parents and both of my grandmothers for their continued support. A special thank you goes to my wonderful girlfriend who has been at my side and has been extremely supportive of me for this entire process. Finally, I would like to thank all of my friends, both at Saint Mary's University, and elsewhere. They have helped to make my continuing journey of learning a positive experience.

Table of Contents

List of Figures   **Page Number**

List of Tables   Page Number

List of Abbreviations and Symbols	**Definition**
MOF	metal-organic framework
CP	coordination Polymer
IUPAC	International Union of Pure and Applied Chemistry
XRD	X-ray diffraction
1D	1-dimensional
2D	2-dimensional
3D	3-dimensional
IR	infrared
π	π-orbital
atm	atmosphere
SIFSIX	hexafluourosilicate
bpe	1,2-bis(4-pyridyl)ethane
syn	same side
POM	polyoxometalate
λ_{max}	wavelength of maximum absorption
NHC(s)	*N*-heterocyclic carbene(s)
HOMO	highest occupied molecular orbital
LUMO	lowest unoccupied molecular orbital
IL(s)	ionic liquid(s)
DFT	density functional theory
TMS-imidazole	*N*-(trimethylsilyl)imidazole
R	reagent

S	solvent
T	temperature
NMR	nuclear magnetic resonance
DMF	*N-N*-dimethylformamide
Å	angstrom, 10^{-10} metres
ATR	attenuated total reflection
FT	Fourier Transform
λ	wavelength

1. Introduction

1.1. Metal-Organic Frameworks
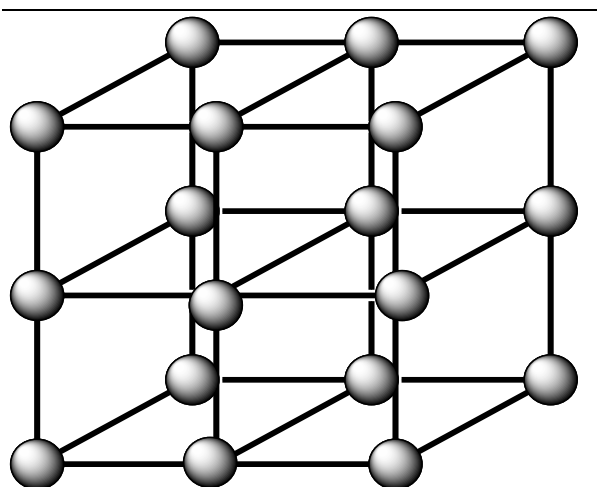
Figure 1: The general structure of a simple MOF. The grey spheres are the metal nodes, and the bold lines are the organic linkers. This structure repeats indefinitely in all directions.

Metal organic frameworks (MOFs), are a subclass of coordination polymer (CP) that usually contain regular voids, channels, or pores, often accessible to solvent, or other molecules. The IUPAC definition is "a metal organic framework (MOF) is a coordination polymer (or alternatively a coordination network) with an open framework containing potential voids."[1] This framework is constructed from metal ions, often referred to as nodes, or connectors, and organic ligands, which are often referred to as linkers.[2] An example of a basic MOF structure is illustrated in Figure 1. This connectivity results in the formation of channels in which guest molecules can reside, providing applications in gas adsorption,[3-5] catalysis,[6] and in special cases, ion exchange.[7,8]

1.1.1. History

The first mention of a coordination polymer in the literature was in a spectroscopic study conducted on a series of cobalt-amine complexes published in 1916.[9] Without single crystal X-ray diffraction (XRD) crystallography, however, there was no way to demonstrate that these compounds were indeed CPs. It was not until 1936 that the structures of Prussian Blue compounds

were demonstrated to consist of an extended 3D coordination network having CN⁻ anions as linkers, and metal ions as the nodes.[10] This was done by a powder XRD technique, and so finer structural details could not be determined.[10] These Prussian Blue compounds were studied in greater detail in 1967, further confirming the older findings.[11] The first single crystal XRD structure of a CP was published in 1949 and consisted of a 2D network of square planar nickel ions linked by CN⁻ anions. Every other nickel atom had an ammonia molecule coordinated at the axial positions, each extending toward the adjacent 2D layers above and below the equatorial plane.[12] Between the 2D coordination networks, benzene molecules were trapped in the cage-like structures that were formed by the extension of the coordinated ammonia molecules.

All the structures mentioned thus far except for some of the early cobalt-amine complexes,[9] are strictly inorganic in nature. The first reported true MOF, that is, one having organic linkers, was reported in 1959 and has the general chemical formula [Cu(abiponitrile)$_2$]·NO$_3$.[13] This compound, and many others similar to it were eventually given the name "metal-organic frameworks" in a publication in 1995 by Yaghi *et al*.[14]

1.1.2. Properties

The properties that a MOF possesses are dependant on many various factors, including those that are structural such as the linker-node combination, dimensionality, coordination number around the node, functionalization of the linker, *etc*. There are also other factors, including thermal conditions (i.e. temperature), identity of guest molecules, and gas pressure that play a role in the properties they possess.[2] One of the key properties that MOFs possess is extremely high surface areas, with values reaching well into the multiple thousands of cm^3/g.[2] This high surface area makes them ideal for heterogeneous applications, as mentioned above.

In general, MOFs are synthesized by combining a solution of the organic linker (the Lewis base) with a solution of the ionic metal node (the Lewis acid). This is done using a variety of techniques such as solvent layering diffusion,[3,4] ionothermal conditions,[15] solvothermal conditions, and hydrothermal conditions. Direct combination of the solutions with simple stirring is also employed in many cases, but does not typically result in the formation of XRD quality crystals.

1.2. Applications of Metal-Organic Frameworks

1.2.1. Gas Adsorption and Separations

A very early example of a MOF that provides much insight into the selective inclusion of guest molecules was reported by Yaghi *et al*. in 1995.[14] The framework reported therein consisted of 1,3,5-tircarboxylatebenzene ligands, each coordinated to three cobalt ions. It was synthesized with the inclusion of pyridine molecules as guests that coordinated to the unsaturated metal centres. Upon removal of pyridine with heating under vacuum, the framework appeared to remain intact, as shown using powder XRD. The researchers then tested the evacuated material for selective adsorption of aromatic species. A typical experiment consisted of suspending the evacuated MOF in binary mixtures consisting of an aromatic solvent and the non-aromatic analogue (e.g. 50/50 mixture of CH_3CN/C_6H_5CN). After filtration, the IR spectra confirmed that the signal arising from the functional group corresponded to being bonded to an aromatic ring. There was also no signal for C-H stretches in the aliphatic region, further bolstering their findings. The reason for this selectivity, in this case, is due to favorable π-π interactions between the aromatic guest molecules, and the 1,3,5-tircarboxylatebenzene linkers of the framework. This work not only illustrated applications for MOFs in chemical separations, but also showed the potential for the development of selective, heterogeneous catalysts (Section 1.2.2).

One of the first examples of gas adsorption was reported by Kitagawa *et al.* in 1999.[16] In this report, the gas being adsorbed was methane, but in order to accomplish this, pressures above 5 atm were required. Given the early stage of development in the field, these were very exciting results, and could still be practical in gas storage applications. The authors attributed their success to having synthesized a MOF that is not an interpenetrated structure. Interpenetration occurs when two frameworks are intertwined *via* linkers penetrating the pores, or channels of the respective partner framework. When this occurs, the size of the channels, and thus the available volume for gas adsorption are greatly reduced. There are, however, cases in which the interpenetrated structure outperforms the non-interpenetrated structure in gas adsorprion. A publication in 2013 by Zaworotko *et al.*[3] describes the synthesis of two MOFs having the same connectivity, with one being interpenetrated, and the other not interpenetrated. Both were tested for the selective uptake of CO_2 in binary gas mixtures with N_2, H_2 and CH_4. The interpenetrated structure outperformed the non-interpenetrated structure, achieving excellent selectivity at just 0.15 bar partial pressure of CO_2. The pore size in the interpenetrated structure, being smaller in size, lead to a pore size that was selective to CO_2 capture. The structure of this framework consisted of a flat, 2D network of 4,4'-dipyridylacetylene linkers coordinated on the equatorial positions of a copper(II) nodes. At the axial positions of the copper atoms, SiF_6^{2-} (SIFSIX) are coordinated, behaving like pillars and linking the sheets together in the third dimension. In a later study, the same interpenetrated MOF was shown to adsorb of C_2H_2 (acetylene) gas with excellent selectivity in mixtures with C_2H_4 (ethylene).[4] The ability for this selective adsorption is attributed to physisorption in the form of C-H$\cdots$F hydrogen bonding of acetylene with the SIFSIX anion pillars, and van der Waals interactions with the 4,4'-bipyridine linkers.[4] Not only was the performance of this MOF outstanding, but it was also moisture and air stable, lending itself to real world applications in gas separation.

1.2.2. Catalysis

When examining the catalytic activity of MOFs, care must be taken to ensure that the catalytic activity of the MOF is not simply due to the constituents of the framework dissolving and acting as a homogeneous catalyst.[17,18] Simple control experiments such as isolating some or all of the supernatant immediately after all the reagents are added to the reaction mixture are typically used to test this potential issue.[18] These sorts of control experiments are not used in all cases, however, and so care must be taken when reading published work in the field, as some results may be deceiving.[18] Some of the main features that make MOFs so attractive as catalysts is their extremely high surface area, the ease of which they can be recycled, due to the simple separation of the solid MOF from the solution, and the tunability of their properties by changing metal-ligand combinations. The catalytic activity in a MOF can be attributed to either coordinatively unsaturated metal centres, the organic linkers used, or combinations of the two.[19]

1.3. Ionic Metal-Organic Frameworks

A subclass of MOFs that is gaining popularity and have a plethora of potential applications are ionic MOFs. These materials are constructed such that there is a net charge on the framework that must be balanced by the presence of counter ions.[8] These ions are typically free in the channels of the framework. There are, naturally, two classes of ionic MOFs; cationic, and anionic, which have positively charged frameworks, and negatively charged frameworks, respectively.[8] There are two general approaches for synthesizing such MOFs. They are referred to as the post-synthetic approach and the pre-synthetic approach. In the post-synthetic approach, a neutral MOF is first synthesized, then it is somehow modified to convert it to an ionic MOF. In the pre-synthetic approach, the original combination of the metal nodes and the organic linkers results in a framework that is already charged, and thus it does not require any further steps to arrive at the

desired product. Of these two approaches, the pre-synthetic is more common, as the planning and procedures are typically more straightforward and require fewer steps to execute. Once synthesized, the ionic MOFs have a number of properties that arise to give them applications in gas adsorption,[8,20-21] catalysis,[8,22-23] non-linear optics,[8] sensing,[8] and ion exchange.[8, 24-25]

1.4. Cationic Metal-Organic Frameworks

1.4.1. Design Strategies

Cationic MOFs consist of a cationic framework that is charge balanced by anions, which are either free in the MOFs' channels, or weakly coordinated to the metal nodes by electrostatic interactions. They have many of the applications mentioned above in the previous section. As outlined in a recent review by Karmakar, *et al.*, there are two distinct pathways for both a post-synthetic approach, and a pre-synthetic approach to cationic MOFs.[8] These are illustrated in Figure 2. Referring to Figure 2, the first approach consists of using a neutral ligand as the linker and combining it with the salt of the metal node, resulting in free anions of the metal salt residing in the channels of the MOF. The second approach uses a cationic ligand as the linker, resulting in the positive charge residing on either just the linker, or the linker and the node, depending on the coordination properties of the anions present. These first two mentioned are broadly used approaches, and thus no specific examples are provided.

In the third approach, a functionalized neutral ligand (i.e. having a functional group in addition to the coordination sites) is used to construct a neutral MOF. In a subsequent step, a reaction is carried out at the functional group, resulting in the generation of a cationic framework.
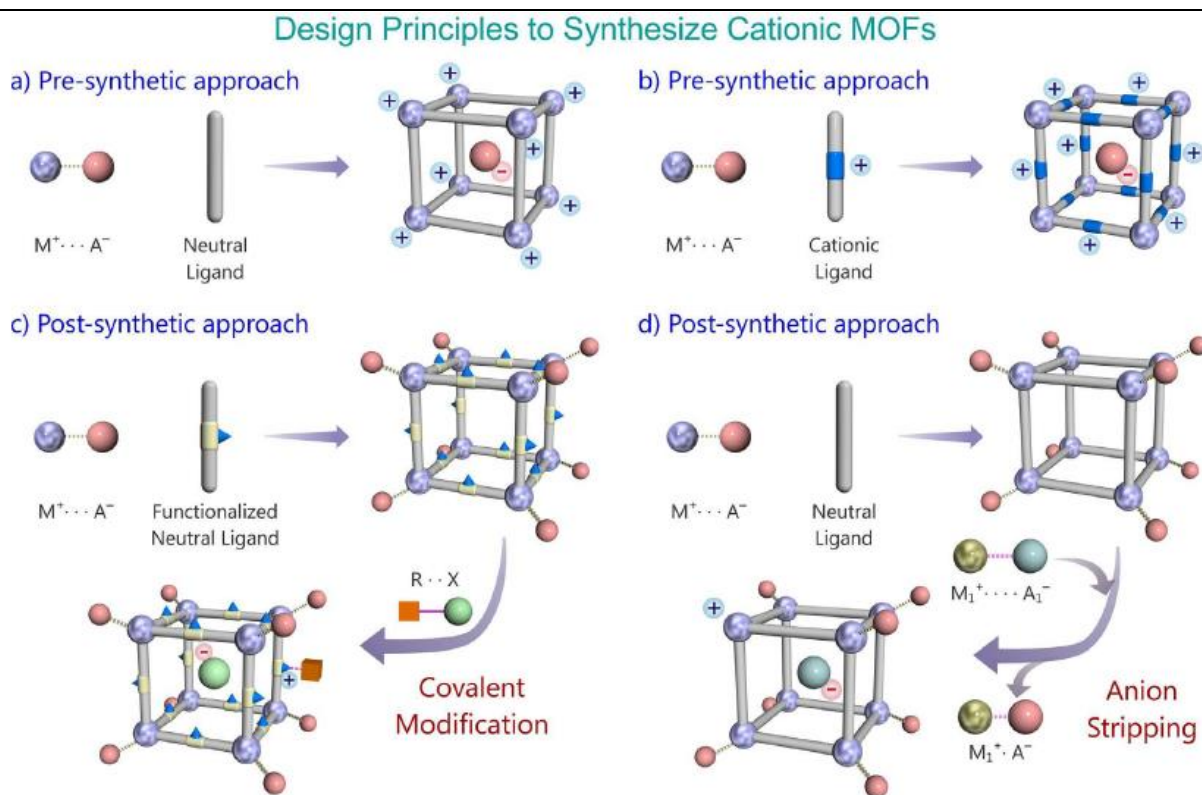
Figure 2: An illustration of the different pathways with which a cationic MOF can be synthesized.[8]

 An early example of this type of synthesis comes from Seo *et al*. where the researchers synthesized a neutral MOF using a pyridine functionalized neutral ligand.[26] The pyridine groups lined the interior of the channels, and could thus be quaternized *via N*-methylation in a subsequent step. To accomplish this transformation, the researchers stirred a suspension of the MOF in *N,N*-dimethylformamide with an excess of iodomethane for 2 hours at room temperature. This afforded the final product, now possessing cationic pyridinium functionality.

In the fourth approach, a more general ion stripping method was published by Mao *et al*.[27] In this method, anions that were strongly coordinated to the metal nodes were stripped and replaced with weakly coordinating/noncoordinating anions. One example of this process uses $AlCl_3$ to strip away the coordinated F^- anions and replace them with non-coordinating Cl^- anions. This exchange

takes advantage of the higher affinity that F^- has for Al^{3+} than for the Cr metal nodes (i.e. $AlCl_3$ is a stronger Lewis acid).

In the pre-synthetic approaches (one and two above) to cationic MOF synthesis, the anion can play a more important role than would be suspected at first glance. A relatively early example of this was published in 2001 by Suresh *et al.*[28] It was found that hydrogen bonding of the ClO_4^- counter anion with water was critical in forcing the 1,2-bis(4-pyridyl)ethane (bpe) ligands they used into the *syn* conformation necessary to form the MOF $\{[Co(bpe)_2(H_2O)_2](ClO_4)_2 \cdot (H_2O)_2\}_n$. When $CoCl_2$ was used instead of $Co(ClO_4)_2$, the hydrogen bonding did not occur, resulting in the MOF not being formed. This idea of using anions to influence the structure of the MOF formation was taken a step further by Wang *et al.*[29] The polyoxometalate (POM) anion $SiW_{12}O_{40}^{4-}$ was used as a template for the channels in the first template synthesized, interpenetrated cationic MOF. The POM allowed for control over the formation of the pores, but unfortunately, it almost completely occupied them. The authors concluded the paper by stating that if the POM could be removed, it would result in a truly porous material. A later study by the same group in which a different MOF was constructed using the same POM revealed that the POM was heavily involved in hydrogen bonds with the framework, and if it were removed, the structure might collapse.[30]

1.4.2. Applications

1.4.2.1. Ion Exchange

A prominent application for cationic MOFs is in anion exchange. A MOF is an attractive material for this application due to the tunabilty of its pore size, as well as the chemical environment within its solvent accessible voids. This ability gives the potential for cationic MOFs to undergo selective anion exchange that could make them potentially superior to other anion

exchange materials. For practical applications, the material must be water stable, and the exchange must be reversible.

A relatively early example of a cationic MOF with reversible anion exchange was demonstrated by Shu *et al*. in 2006.[24] In this example, the MOF formed with ClO_4^- ions present in the channels. It was found that they could be fully exchanged with NO_3^- ions by submerging the crystals in an aqueous solution of $NaNO_3$. To test the reversibility of this exchange, the NO_3^- occupied version of the MOF was submerged in an aqueous solution of $NaClO_4$, which revealed that full exchange of the anion had taken place. This all occurred without any damage to the structure of the framework, as evidenced by powder XRD of the test samples. In addition to reversibility, selective exchange of anions has also been demonstrated in a study by Ghosh *et al*. in 2016.[25] A cationic MOF was synthesized, and in water, it was able to exchange its free SO_4^{2-} anions for $Cr_2O_7^{2-}$, a common and harmful waste product of industry.[25] It was also able to exchange with MnO_4^-, which serves as a model for the anion TcO_4^-, common in radioactive waste. To test the selectivity, the crystals were added to a series of aqueous solutions containing either MnO_4^-, or $Cr_2O_7^{2-}$ in a series of binary mixtures with ClO_4^-, NO_3^-, BF_4^-, or $CF_3SO_3^-$ ions. As shown by FT-IR of the crystals, the uptake of MnO_4^- and $Cr_2O_7^{2-}$ was selective over the other ions tested. Although high capacity for ion exchange is desirable, in practical applications, selectivity is more desirable as this prevents the materials from becoming quickly saturated with anions that are of no interest.

1.4.2.2. Sensing

Another interesting and promising application that is emerging for cationic MOFs is in their use as sensors.[8] This application has become a very attractive and enticing area of research due to the high diversity in the structures that can be obtained by varying the metal-ligand

combinations. These combinations can be optimized to have interactions with different guest molecules, such that a change in the properties of the MOF can be detected in the presence of target molecules.

In an example from 2011, a cationic MOF that was able to sense solvent vapours was reported by Zhang *et al*.[31] This MOF was synthesized using a Zn(II) salt and rigid, heteroaromatic ligands containing nitrogen atoms through which it coordinated. The structure was such that once synthesized, there were free nitrogen atoms lining the interiors of the channels, which was the key to the sensing ability of the MOF. In the presence of different solvent vapours, the absorbance properties of the MOF were drastically changed; that is, λ_{max} was shifted significantly. This gave the ability to determine the identity of various solvent vapours with the assistance of UV-Vis absorption measurements.

Cationic MOFs are also highly useful in the detection of components in aqueous media such as anions, and can also possess other desirable properties simultaneously, making for a multifunctional material. In one such example reported by Sun *et al*. in 2015, a series of three cationic MOFs were synthesized such that the only difference between them was the ligand used.[32] These MOFs were all able to be used as sensors for lanthanoid(III) (Ln^{3+}) ions, particularly Tb^{3+} *via* the ion's luminescent properties when protected inside the pores of the MOF. The selective sensing of common environmentally harmful CrO_4^{2-} and $Cr_2O_7^{2-}$ ions was also possible by the naked eye *via* a colour change. The MOFs also demonstrated the ability to adsorb toxic organic dyes that could then be released, allowing the MOFs to be reused in the application.

1.5. *N*-Heterocyclic Carbenes and Their Corresponding Azolium Salts
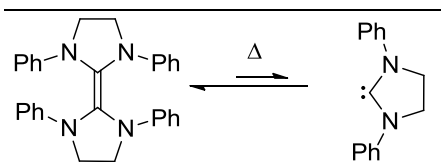
Figure 3: The generation of an NHC by heating the dimer.

N-heterocyclic carbenes (NHCs) are a special type of carbene that bares its lone pair of electrons on a carbon atom that is adjacent to (a) nitrogen atom(s) in a *N*-heterocycle.[33] The first descriptions of this class of compound appeared in the early 1960s, but due to the unstable nature of these species, the reactivity and other properties had to be explored by generating the carbene *in situ*. This was done by heating the corresponding dimer, as shown in Figure 3.[33] In 1962, a paper[34] published by Wanzlick demonstrated the reactivity of imidazolylidenes toward various electrophiles, and also showed that the corresponding imidazolium salts are acidic enough to slowly exchange with D_2O in an NMR experiment. Soon after this, Wanzlick reported the first carbene metal complex in 1968.[35] It was not until 1991 that the isolation of the first stable, free NHCs were reported by Arduengo *et al.* (Figure 4).[36]
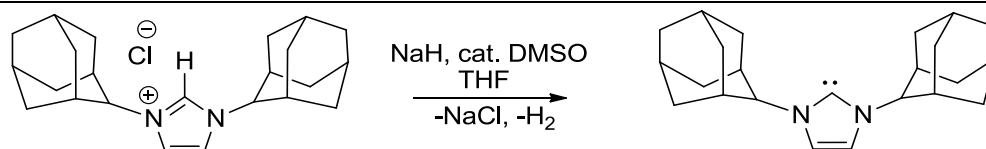
Figure 4: The preparation of one of the first stable NHCs as reported by Arduengo *et al.*[36]

When compared with other carbenes, NHCs are unusually stable, and there are now many examples that can be stored indefinitely under the proper conditions.[33] The stability of an NHC can be explained by the steric bulk of the *N*-substituents, as well as its electronic properties. This is due to the donation of electron density into the empty *p*-orbital of the carbene from the lone pairs on the neighbouring nitrogen atoms, making the carbene less electrophilic. In turn, there is also an inductive electron withdrawing effect of the more electronegative nitrogen atoms, which makes the carbene lone pair less electron dense, and therefore less nucleophilic. The electronic

configuration of the carbene is also important, since triplet carbenes are generally less stable,[37] and cannot readily accept electron density into their *p*-orbitals the way that singlet carbenes can (Figure 5). Triplet NHCs are rare, if they exist at all, since the π-donation shown in Figure 5a is not possible, due to the occupation of the accepting orbital (Figure 5b).
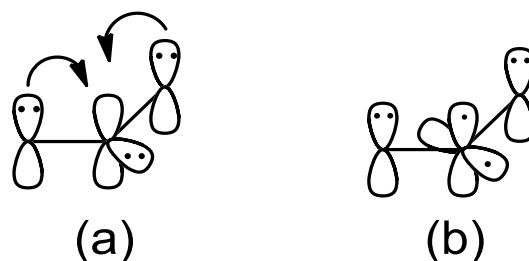
Figure 5: The orbital configuration of a singlet NHC (a) compared to that of a triplet NHC (b).

1.5.1. *N*-Heterocyclic Carbene Metal Complexes

NHCs have become very popular ligands in transition metal, and organometallic chemistry. This is due to the stability of the complexes they form, and their strong electron donating abilities. It was initially thought that NHCs were purely σ donors, but more recent studies on their complexes have found otherwise. A result published in 2001 showed a shorter than expected C-Cu bond length in a Cu(I) NHC complex.[38] This result indicates that there is some π back-bonding, and so the interaction is not purely σ donation. Later, in 2004, the contribution from π back-bonding was calculated to be approximately 20% in group 11 metals.[39] The applications of NHC metal complexes are mostly in catalysis, such as in olefin metathesis,[40] and in palladium catalysis.[41,42]

1.5.2. *N*-Heterocyclic Carbene Copper (II) Complexes

Although Cu(I)-NHC complexes are common,[33,43,44] Cu(II)-NHC complexes are much less common due to their inherent instability, which can be explained by hard-soft acid-base theory.[44] Carbon is a soft donor ligand, and so its HOMO overlaps well with the LUMO of the soft acceptor,

Cu(I). Cu(II), however, is considered an intermediate/hard acceptor, and so orbital overlap is poor, leading to lower stability. To stabilize these complexes, most examples make use of NHC ligands that contain a negatively charged substituent, usually an alkoxide, or phenoxide on one, or both nitrogen atoms. This hard donor, which coordinates to the Cu(II) centre, stabilizes the complex, allowing for their isolation.[44-46] There are however, some examples in which pyridyl and/or picolyl *N*-substituents are put in place of the negatively charged substituent, offering a similar stabilizing effect, without the anionic tether.[44] The copper (II) NHCs exhibit similar, and in some cases, enhanced catalytic activities over the copper (I) NHCs, making them of high interest.[44-46]

To synthesize these complexes, silver-NHC transfer reagents, or other NHC transfer reagents are typically used, resulting in the need for more steps to arrive at the final product.[44,47] This procedure could possibly be streamlined by eliminating the requirement for the use of an NHC transfer reagent in the first place.

1.6. Target Compounds for Metal-Organic Framework Synthesis

1.6.1. Imidazolium Ligands

The desired ligands for the construction of the cationic MOF are 1,3-bis(pyridin-3-ylmethyl)imidazolium and 1,3-bis(pyridin-4-ylmethyl)imidazolium in various salts.

The rationale for the design of these ligands is that they can coordinate through the nitrogen atoms of the pyridine rings to form a coordination polymer, and they consist of the positively charged, imidazolium core; potentially enhancing such a MOF for CO_2 capture *via* chemisorption onto the C2 position of the imidazolium core.
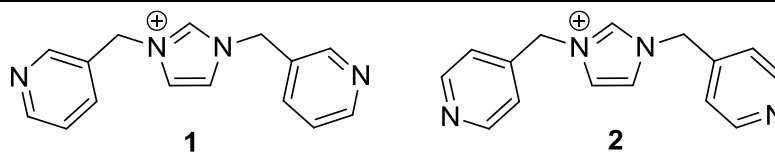
Figure 6: 1,3-bis(pyridin-3-ylmethyl)imidazolium (**1**) and, 1,3-bis(pyridin-3-ylmethyl)imidazolium (**2**).

For imidazolium acetate ionic liquids (ILs), a possible mechanism for this chemisorption is shown in Figure 7.[48] Since the acetate, which is the counter anion in this case is basic, there lies an equilibrium between the imidazolium salt, and the free NHC. In the presence of CO_2, a 2-carboxylate-NHC adduct will form, trapping the CO_2. If this adduct is heated, the CO_2 will be liberated, and the free NHC will be regenerated,[33] making the process potentially reversible.
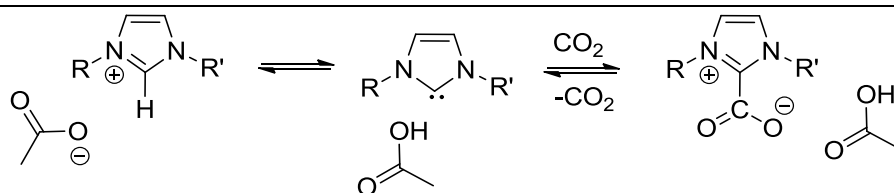
Figure 7: A possible mechanistic pathway for CO_2 chemisorption of acetate ILs.

In addition to chemisorption of CO_2, imidazolium salts have also been shown to catalyze the production of cyclic carbonates from the reaction of CO_2 and an epoxide, but many of the earlier examples of this chemistry required relatively high pressure.[49] Instead of using free ILs as homogeneous catalysts, heterogeneous systems can be designed by grafting the imidazolium moieties onto a polymer support.[50,51] This increases the stability of the catalyst, and makes recycling more straight forward.[50,51] A paper by Wang *et al.* published in 2015 nicely illustrates a multifunctional material possessing the ability to capture CO_2 and to catalyze the formation of cyclic carbonates.[50] This material consists of a porous hyper-crosslinked polymer that is functionalized with imidazolium salt moities.[51] The crosslinked backbone consists of a phenyl ring

network that was synthesized by Friedel-Crafts alkylation between benzyl chloride molecules. The network was then treated with *N*-methylimdazole, which displaced the chloride, resulting the final product. The material was able to convert CO_2 to cyclic carbonates when treated with various epoxides with excellent yields, and it also displayed good CO_2 uptake capacity. Using 1-methyl-3-benzylimidazolium chloride as a model compound, Zhang and co-workers investigated the mechanism of this conversion using density functional theory (DFT) calculations, with the proposed mechanism shown in Figure 8.[50]
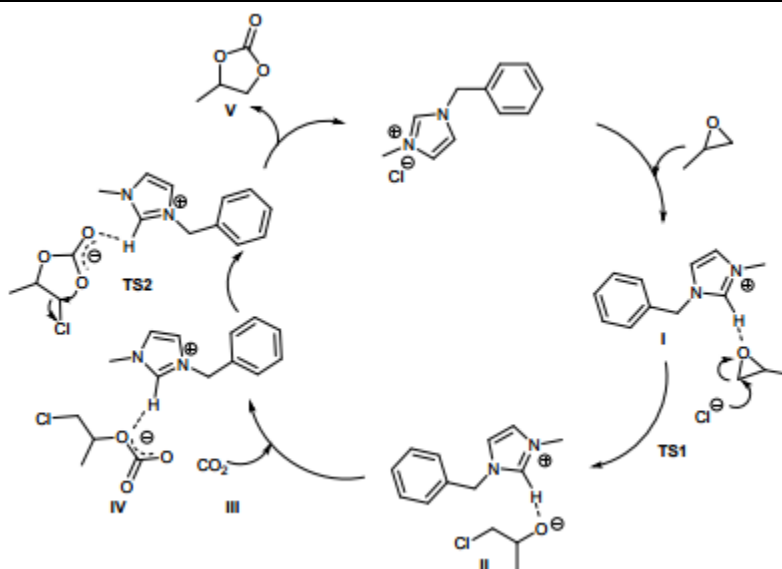
Figure 8: The mechanistic pathway for imidazolium catalyzed CO_2 conversion based on DFT calculations proposed by Wang *et al.*[50]

When this material is compared to polystyrene (PS) supported imidazolium chloride, the porous polymer performs much better when the pressure is reduced. This is because within the pores of the material, even at lower pressures, the CO_2 concentration remains high around the catalytic site, giving this heterogeneous catalyst a distinct advantage over the PS supported catalysts.

The ligand 1,3-bis(pyridin-2-ylmethyl)imidazolium chloride has already been demonstrated to form CPs, with silver ions,[52] and tridentate NHC metal complexes with

palladium.[38] Given its similarities to the proposed ligands, **1** and **2** they are justified for the construction of a MOF for CO_2 adsorption.

1.6.2. SIFSIX Materials

The SIFSIX anion (SiF_6^{2-}) is one of the key components in some of the best gas adsorption materials that have been developed to date.[3,4,53] As already mentioned in Section 1.2.1, these anions contribute immensely to the internal environment of the pores, facilitating highly favourable interactions with guest molecules, resulting in physisoprtion. The SIFSIX anion also behaves as a structural pillar in the third dimension for these materials, giving them enhanced stability and rigidity.

1.7. The Proposed Material and Hypothesis

The compounds 1,3-bis(pyridin-3-ylmethyl)imidazolium (**1**) and, 1,3-bis(pyridin-3-ylmethyl)imidazolium (**2**) are to be used in combination with $CuSiF_6$ to construct cationic MOF materials. The structure and structural features of the proposed materials will be elucidated by the utilization of single crystal XRD analysis. It is proposed that if successfully prepared, these materials will possess enhanced CO_2 adsorption properties by combining the chemisorption of imidazolium salts, and physisorption and pore size control of the SIFSIX anions. In particular, the Cu(II) SIFSIX salt will be used primarily due to the good HOMO/LUMO matching of Cu(II) with pyridine, and the previous success by others using this salt.[3,4] Given the cationic nature of the proposed materials, they might also possess the ability to perform catalysis and/or ion exchange.

1.8. Concluding Remarks on Cationic MOFs

Cationic MOFs have demonstrated many of the applications that their neutral counterparts have, and have some added applications due to their anion exchange properties. They also have the potential for improved chemical sensing arising from their unique electronic properties.
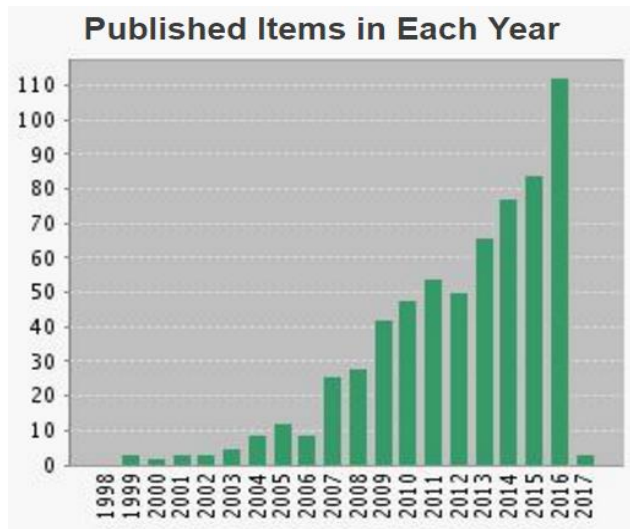
Figure 9: Research articles (only) published per year for the search "cationic AND metal organic framework" in Web of Science.

The field of research is one that has been rapidly growing, as shown in the graph (shown in Figure 9). As more focus is being aimed toward researching the structure, properties, and applications of the cationic MOFs, there is the potential for their widespread use in some, or all of the applications that are currently being developed.

2. Results and Discussion

2.1. Synthesis of 1,3-bis(pyridin-2-ylmethyl)imidazolium chloride (3), *N*-(pyridin-3-ylmethyl)imidazole (4)

To synthesize **3**, a procedure that was modified from the literature was used on a reduced scale.[38,52] 2 equivalents of 2-(chloromethyl)pyridine hydrochloride, 1 equivalent of imidazole, and 3.1 equivalents of sodium bicarbonate were taken up in ethanol, and held under reflux for 48 hours. After workup, **3** was obtained in a 57 % yield. From a reaction following the scheme in entry 5 of Table 1, the intermediate **4** was isolated from the tetrahydrofuran (THF) that was used to triturate

the solids. It was initially a yellow oil, that over the course of several weeks, formed crystals in the vial in which it was stored. Although not ionic, this compound still had the useful structure to form CPs.
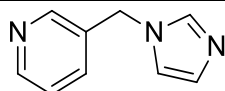
Figure 10: The structure of *N*-(pyridin-3-ylmethyl)imidazole (**4**).
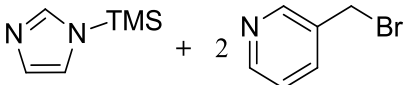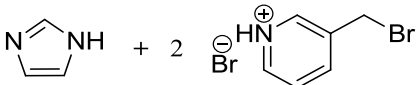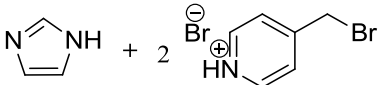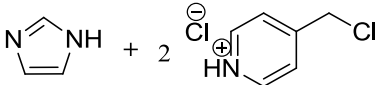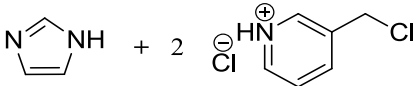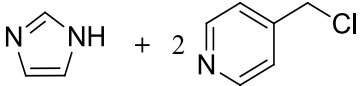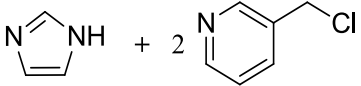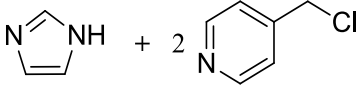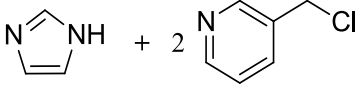
2.2. Synthesis of 1,3-bis(pyridin-3-ylmethyl)imidazolium (1) and 1,3-bis(pyridin-4-ylmethyl)imidazolium (2)
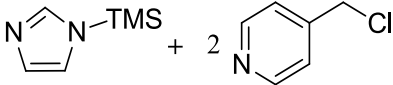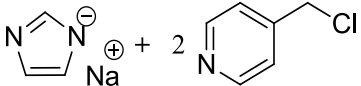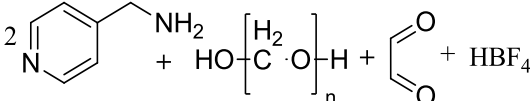
To synthesize both the **1** and **2**, a simple one-step, nucleophilic substitution reaction was attempted with *N*-(trimethylsilyl)imidazole (TMS-imidazole), as shown in entry 1 of Table 1. Since both 3 and 4-(bromomethyl)pyridine were only available as the hydrobromide salts, the free base was first prepared *in situ* by treating an aqueous solution of the salt with either ammonium or sodium hydroxide and immediately extracting it into dichloromethane. This solution was slowly added to a concentrated solution of TMS-imidazole, which afforded a red precipitate after stirring overnight. Both the ^{1}H NMR and ^{13}C NMR spectra indicated a mixture of several compounds that were possibly polymeric in nature had formed. Although separations were attempted, these were unsuccessful.

Entries 2-5 of Table 1 were based on procedures from the literature for the preparation of 1,3-bis(pyridin-2-ylmethyl)imidazolium chloride/bromide.[38,52,54] These methods were straightforward, involving the mixing of the picolyl halide salt, imidazole, and either sodium carbonate, or sodium bicarbonate in excess in the given reaction solvent under reflux conditions. The results for the crude product were slightly better than what was obtained for entry 1, but the NMR spectra still showed a complex mixture. Purification was attempted by repeating the process

of dissolving the mixture in minimal methanol and dropping it into diethyl ether to afford a

precipitate. The process showed little to no improvement as it was iterated.

Table 1: All synthetic approaches that were attempted for the imidazolium core target ligands

Entry #	Reactants and Molar Ratio	Reaction Conditions	Time/h
1		S†: CH_2Cl_2 T‡: Room Temperature	22
2		R*: Na_2CO_3 (4 eq), S: CH_3CN T: Reflux	18
3		R: Na_2CO_3 (4 eq), S: CH_3CN T: Reflux	18
4		R: $NaHCO_3$ (3.1 eq), S: EtOH T: Reflux	48
5		R: $NaHCO_3$ (3.1 eq), S: EtOH T: Reflux	48
6		R: NaH (1 eq), S: DMF T: 110°C, Microwave	2-4
7		R: NaH (1 eq), S: DMF T: 110°C, Microwave	2-4
8		R: NaH (1 eq), S: CH_3CN T: 80°C, Microwave	2-4
9		R: NaH (1 eq), S: CH_3CN T: 80°C, Microwave	2-4

Entry #	Reactants and Molar Ratio	Reaction Conditions	Time/h
10	(imidazole)N–TMS + 2 (pyridin-4-yl)CH$_2$Cl	S: CH$_3$CN T: 80°C, Microwave	2-4
11	(imidazolide)N$^-$⊕Na + 2 (pyridin-4-yl)CH$_2$Cl	S: THF, T: Reflux	22
12	2 (pyridin-4-yl)CH$_2$NH$_2$ + HO$\left[\text{C}^{\text{H}_2}\cdot\text{O}\right]_n$H + (glyoxal) + HBF$_4$	S: Toluene, T: 0-50°C	12

* R=reagent(s), [†] S=solvent, [‡] T=temperature.

Entries 6-9 in Table 1 were attempts to reproduce a literature preparation for 1,3-bis(pyridin-4-ylmethyl)imidazolium chloride involving the use of a pressure tube and sodium hydride, requiring the exclusion of moisture.[55] Lacking access to a pressure tube setup, the reaction was carried out in a sealed microwave tube with microwave heating. The results for both the synthesis of 1,3-bis(pyridin-3-ylmethyl)imidazolium chloride and 1,3-bis(pyridin-4-ylmethyl)imidazolium chloride were better than the results obtained for the previous methods attempted. Although the NMR spectra indicate the product had formed, there was a major impurity present, giving rise to a signal at 2.7 ppm in the ^{1}H NMR (Figure 11) and at 35.4 ppm in the ^{13}C NMR (Figure 12) for the trials using *N-N*-dimethylformamide (DMF). After multiple attempts at purification by trituration with diethyl ether, tetrahydrofuran, and by recrystallizations from methanol vapour diffusion with diethyl ether, this impurity could not be removed. Silica gel flash chromatography was attempted, but the product became irreversibly adsorbed to the stationary phase, even after removing it from the column and extracting with acetonitrile, methanol, water, and even aqueous

base and acid. The contamination peak in both the ^{1}H NMR and ^{13}C NMR spectra match what is observed for dimethylamine hydrochloride, which are reported to be 2.7 ppm in the ^{1}H NMR spectrum and 35.6 ppm in the ^{13}C NMR spectrum.[56] The origin of this contaminant is suspected to be a decomposition product of DMF, which is observed to form in the presence of sodium hydride and heating.[57] The hydride can act as a nucleophile, attacking DMF which prompts its decomposition. The design of the microwave tubes used made the exclusion of moisture from the system extremely difficult, and so any moisture present was converted to sodium hydroxide, which is known to increase the rate of decomposition of DMF into CO and Me_2NH. Similar conditions in acetonitrile lead to poorer results, as acetonitrile can suffer from similar problems with sodium hydride.[57]
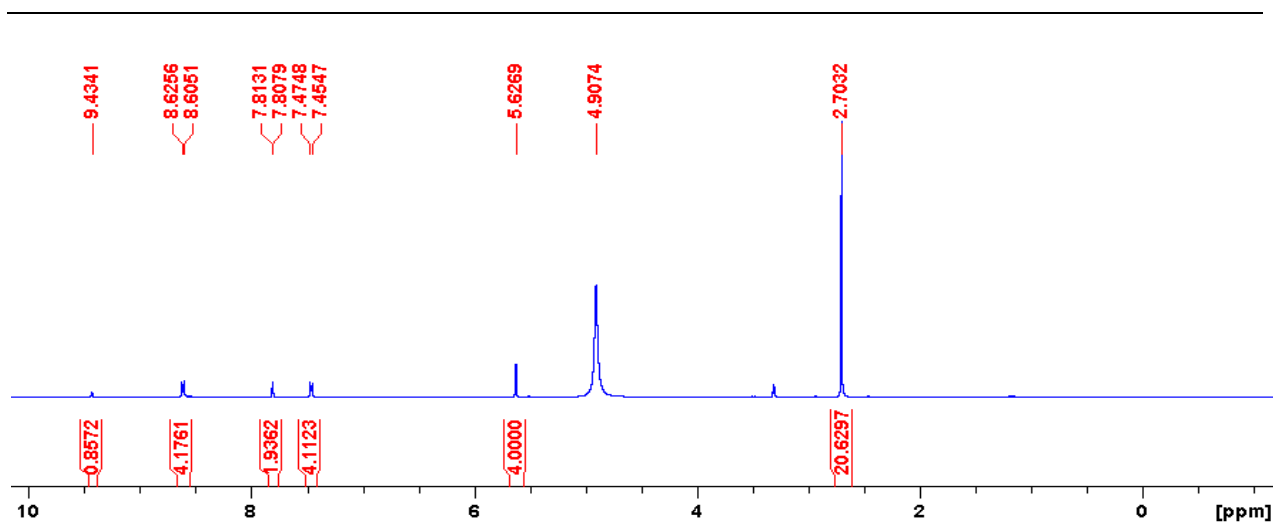
Figure 11: ^{1}H NMR spectrum of 1,3-bis(pyridin-4-ylmethyl)imidazolium chloride in CD_3OD. The broad peak at 4.9 ppm is water (present due to the hygroscopic nature of the substance), and the peak at 2.7 ppm arises due to the contaminant that could not be removed.

Compounds **1** and **2** containing the impurity were attempted in the synthesis of the MOF without further purification, but upon combing with the Cu-SIFSIX by either solvent layering diffusion, or direct mixing in solution, a brown powder that could not be crystallized was obtained.
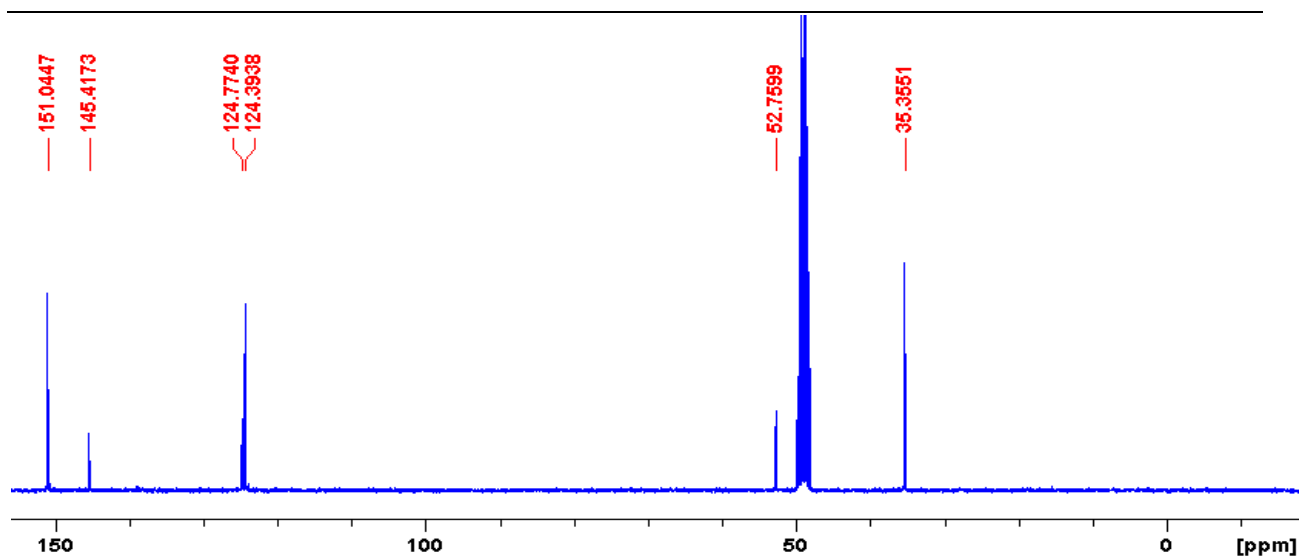
Figure 12: ^{13}C NMR spectrum of 1,3-bis(pyridin-4-ylmethyl)imidazolium chloride in CD$_3$OD. The peak at 35.6 ppm arises due to the contaminant that could not be removed.

In an attempt to circumvent these issues, the sodium hydride and imidazole was substituted for TMS-imidazole (Table 1, entry 10). The results of this attempt were significantly worse than those obtained in Table 1, entries 6-9. It is suspected that although a convenient reagent, TMS-imidazole is a poorer nucleophile than sodium imidazolide, which results in a slower reaction with the first equivalent of electrophile.
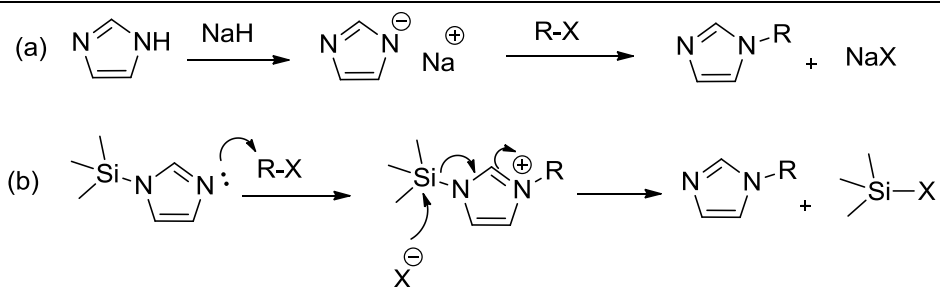
Figure 13: (a) The reaction mechanism of imidazole with an electrophile in the presence of sodium hydride and (b) the reaction mechanism of TMS-imidazole with and electrophile.
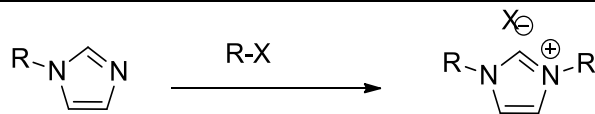
Figure 14: The reaction of the intermediate imidazole with an electrophile, R-X.

For the intermediate produced in Figure 13, the reaction with a second equivalent of electrophile will be at the same rate for the reaction conditions used here. In an attempt to avoid the solvent issues, and still take advantage of the reactivity of the imidazole/NaH mixture, imidazole was stirred with NaH in THF for 30 minutes, then a THF solution of the free base was slowly added under inert atmosphere, then the resulting mixture was brought to reflux. This also resulted in a product that could not be purified.

The main problem with these synthetic methods is the instability of the active free based electrophiles. They can undergo self reaction under the S_N1 and S_N2 reaction conditions by means of the lone pair on the pyridine nitrogen attacking the electrophilic carbon atom of another molecule, eventually forming a polymer (Figure 15). The nucleophilic nitrogen atom can be from any of the species that are present in the reaction mixture already, including any intermediates, the final product, or any polymers/oligomers that have formed. In the first step of the reaction (Figure 11), this polymerization is slow in comparison, and so this explains why *N*-(pyridin-3-ylmethyl)imidazole could be isolated with relative ease. In the second step, however (Figure 14), the unsubstituted nitrogen atom on imidazole should have similar reactivity to that of pyridine. This is where the polymerization becomes a significant issue.
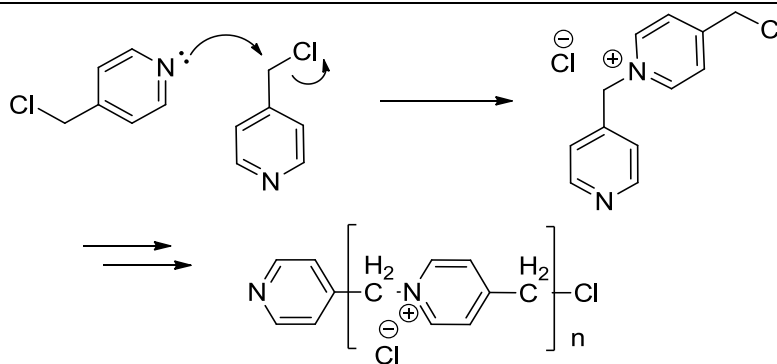
Figure 15: An example of the possible side reactions that can occur when using 4-(chloromethy)pyridine.

For the synthesis of 1,3-bis(pyridin-2-ylmethyl)imidazolium chloride, the polymerization was not an issue for two main reasons: 1) the position of the nitrogen atom on the pyridine ring is sterically hindered by the chloromethyl substituent, and 2) the final product was not hygroscopic, and possessed more diverse solubility allowing for simple purification.
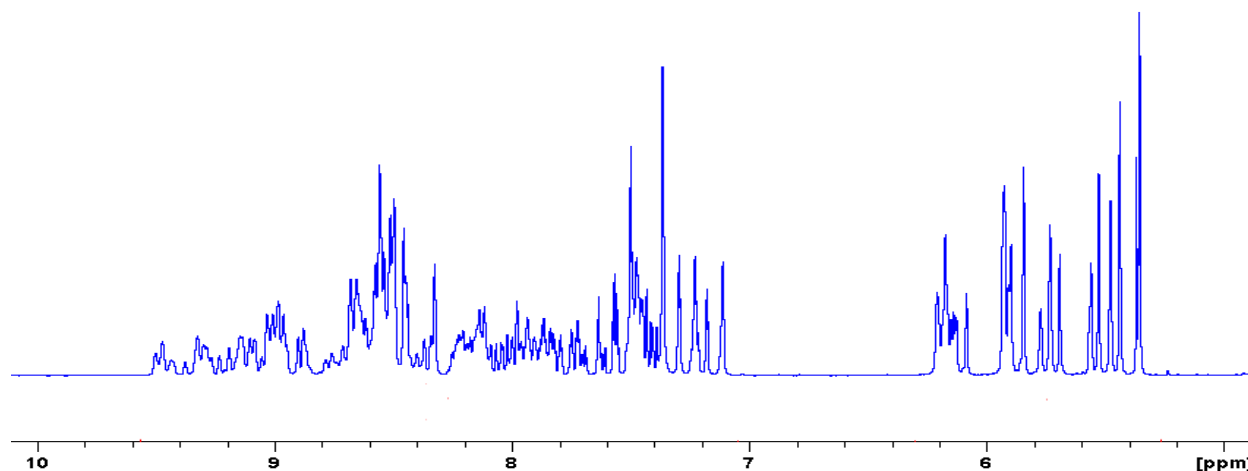
Figure 16: The ^{1}H NMR spectrum of a sample in D$_2$O that is suspected to be polymerized. The reaction type of its origin is that of entry 1 in Table 1.

The conditions described in Table 1, entry 12 were used in an attempt to avoid self reacting picolyl halides all together, and to construct the imidazolium ring with the desired functionality

already built in. This procedure involved first mixing 1 equivalent of the amine (typically an aryl or benzyl amine) with 1 equivalent of paraformaldehyde in toluene. After cooling on ice, the second equivalent of the amine is added, followed by the slow addition of aqueous tetrafluoroboric acid. After warming to room temperature, aqueous glyoxal was slowly added, and the mixture was heated to 50 °C overnight. The solid was isolated by filtration, then recrystallized. When the attempt was made using 4-(aminomethyl)pyridine in place of benzylamine, the addition of tetrafluoroboric acid caused a sticky white precipitate to form. As soon as the addition of glyoxal was started, this solid started turning orange, which quickly intensified to dark red. A red powder was eventually isolated, but the ^{1}H NMR indicated that this solid was by no means pure.
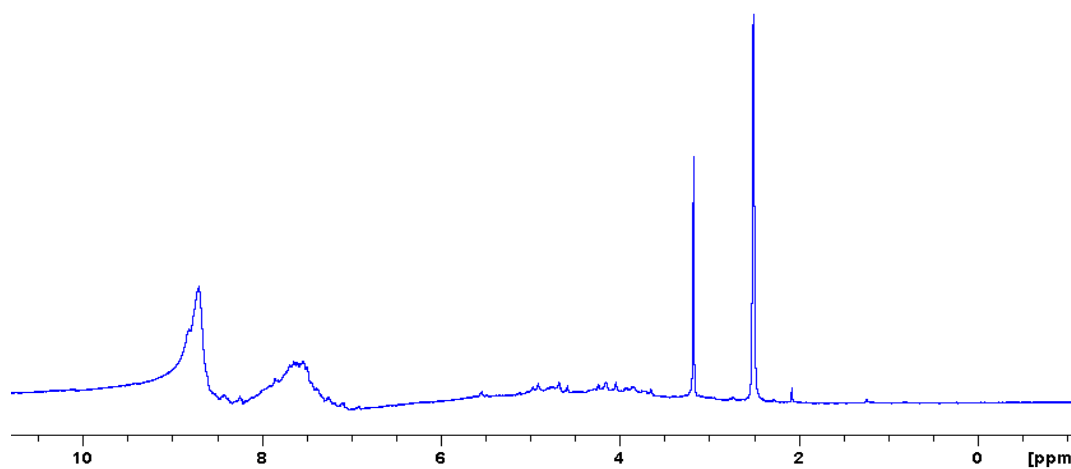
Figure 17: The ^{1}H NMR spectrum of the red crystalline powder that was isolated using the reaction scheme in entry 12 of Table 1 (attempted synthesis of **2**).

This method has been utilized for the convenient preparation of 1,3-dibenzylimidazolium tetrafluoroborate and 1,3-bis(cyclohexyl)imidazolium tetrafluoroborate by using benzylamine and cyclohexylamine, respectively.[58,59] The likely reason that this reaction was unsuccessful for the synthesis of **2**, using 4-(aminomethyl)pyridine is once again the nitrogen atoms of the pyridine ring contributing to extra reactivity, and/or solubility issues.

2.3. Synthesis and Characterization of the Coordination Complexes 5-8

2.3.1. {Cu(II)[(OH₂)₂(*N*-(pyridin-3-ylmethyl)imidazole)₂]-Cu(II)[(SiF₆²⁻)₂(*N*-(pyridin-3-ylmethyl)imidazole)]}ₙ (5)

5 was synthesized by combining a methanol solution of 4 with a methanol solution of CuSiF$_6$·H$_2$O, which immediately formed a precipitate. After washing with several portions of methanol, the powder was dried in air, dissolved in water, and allowed to undergo vapour diffusion with acetone. After approximately 2 weeks, blue coloured plate crystals, suitable for XRD analysis were obtained. The crystal structure revealed that 5 had crystallized in the centrosymmetric monoclinic space group P2$_1$/c. The crystal was twinned, having the twin law -1, 0, 0, 0, -1, 0, 0, 0, 1, with a BASF refining to 0.444. The structure consists of a 1D coordination polymer having 4 ligands coordinating to each copper atom on the equatorial positions. The occupation of the axial positions alternated between SIFIX anions, and water molecules. This is shown in Figure 18.
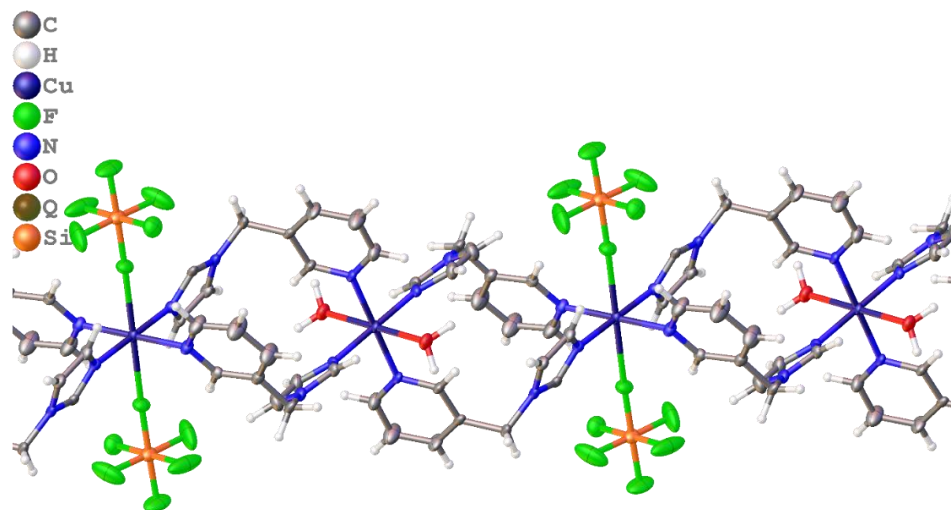
Figure 18: A view of the polymeric chain of 5, showing the alternating coordination sphere around copper. All disordered solvent molecules are omitted for clarity.

 Each coordinated water molecule is involved in a hydrogen bond with the coordinated SIFSIX anion of the neighbouring chain, having an O-F distance of 2.7339(3) Å, an O-H distance of 0.91292(8) and an H···F distance of 1.8905(2) Å (Figure 19). This shows the ability for the SIFSIX anion to form hydrogen bonds.
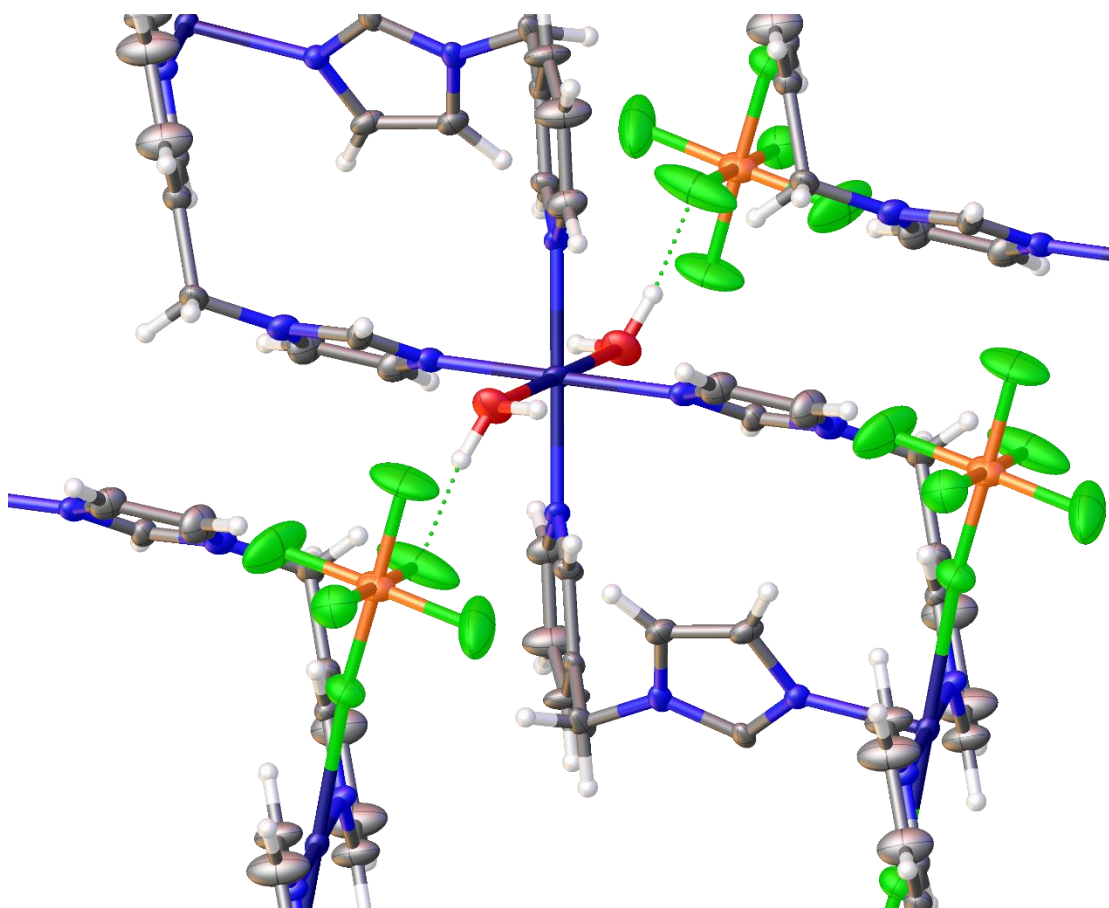
Figure 19: A view of the cross-linking hydrogen bonding in **5**. The thermal ellipsoids are drawn at the 50% probability level.

The chains stack together to form channels that are occupied by severely disordered solvent molecules (likely water, the crystallization solvent). The distances across the channels (calculated using centroids), are approximately 5.87 Å from one pyridine ring to the other, and 4.60 Å from one imidazole ring to the other. These channels are shown in Figure 20.
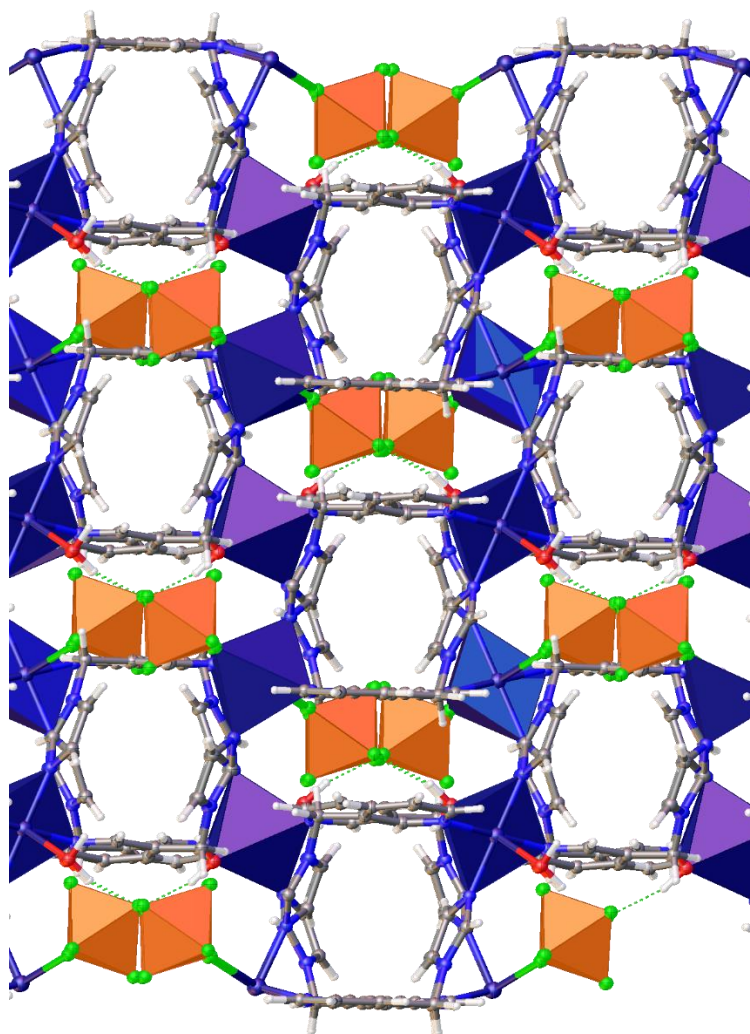
Figure 20: The view down the solvent accessible channels of **5**. The purple octahedrons are the copper atoms, and the orange octahedrons are the SIFSIX anions. The disordered guest molecules are omitted for clarity.

The geometry around each copper atom (Figures 21 and 22) is distorted octahedral. The distortion, which is caused by the Jahn-Teller effect, is common in Cu(II) complexes. This is a result of Cu(II) being a d^9 metal. The type of distortion observed for both Cu1 and Cu2 in **5** are elongation, where the d_z^2 and $d_{x^2-y^2}$ lose their degeneracy and are split such that $d_{x^2-y^2}$ is higher in energy than d_z^2, resulting in lengthening of the axial ligand-copper bond. The bond lengths, which

are shown in Table 2, indicate this distortion is quite severe, with a maximum difference in bond length between axial and equatorial ligands of 0.5071(2) Å. The axial bond lengths are 2.4785(2) Å for the oxygen donor, and 2.4954(2) Å for the fluorine donor. Any distance between a copper atom and an oxygen, nitrogen, or fluorine atom of up to 2.4 Å is typically considered to be a covalent bond.[60] All the equatorial ligands in **5** fall well within this range with bond lengths near 2.0 Å (Table 2). When the copper-ligand distance is in the range of 2.4-2.8 Å for oxygen, nitrogen, or fluorine donors, the interaction is typically considered to be electrostatic in nature.[60] The axial bond lengths for both Cu1 and Cu2 are at the short end of this range, and likely represent strong electrostatic interactions. The bond angles, although deviating from the ideal octahedral angles (i.e. 90 °), are all well within the acceptable range for an octahedral complex (Table 3).

Table 2: Selected bond lengths for 5.

Bond	Length/Å	Bond	Length/Å
Cu1-O1	2.4785(2)	Cu2-F1	2.4954(2)
Cu1-N2	1.9771(2)	Cu2-N5	1.9883(2)
Cu1-N6	2.04877(14)	Cu2-N3	2.04412(18)

Table 3: Selected bond angles for 5.

Bonds	Angle/°	Bonds	Angle/°
O1-Cu1-N2	86.817(6)	F1-Cu2-N5	89.796(6)
O1-Cu1-N6	88.879(9)	F1-Cu2-N3	87.928(10)
N2-Cu1-N6	86.432(5)	N3-Cu2-N5	87.422(5)
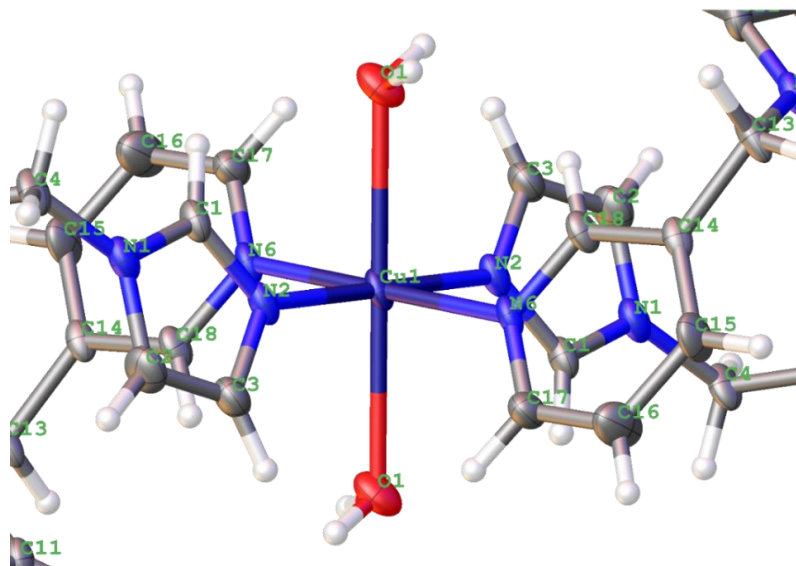
Figure 21: The coordination environment around Cu1 of **5**.
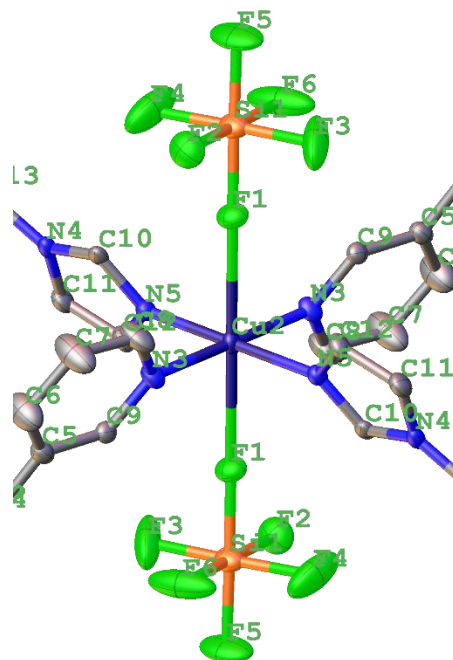
Figure 22: The coordination environment around Cu2 of **5**. All hydrogen atoms have been omitted for clarity.

2.3.2. Cu(1,3-bis(pyridin-2-ylmethyl)imidazolylidene)(MeOH)$_2$(SiF$_6$$^{2-}$) (6)

3 has been shown to form coordination polymers with Ag$^+$ in a previous report,[52] and since the synthesis of **1** and **2** were unsuccessful, an attempt at synthesizing a MOF was made by combining **3** with Cu-SIFSIX. With no precaution to exclude moisture, a methanol solution of CuSiF$_6$·H$_2$O was combined with a methanol solution of **3**. After stirring overnight at room temperature, a fine blue precipitate had formed, which was slightly soluble in methanol. Crystals that were suitable for single crystal XRD were obtained after 1 week of vapour diffusion of chloroform into a methanol solution of **6**. Single crystal XRD analysis revealed that **6** had crystallized in the non-centrosymmetric, orthorhombic space group, Pna2$_1$. After refinement of the model while applying the MOVE 1 1 1 -1 command to invert the configuration, the R1 value had increased from 3.09% to 5.29%, the Flack parameter had changed from 0.005(6) to 0.996(6) and Olex^2 gave a warning indicating that the structure should be inverted back. The Flack parameter of 0.005(6) and the poorer refinement obtained for the inverted structure both indicate that **6** crystallized with absolute configuration.
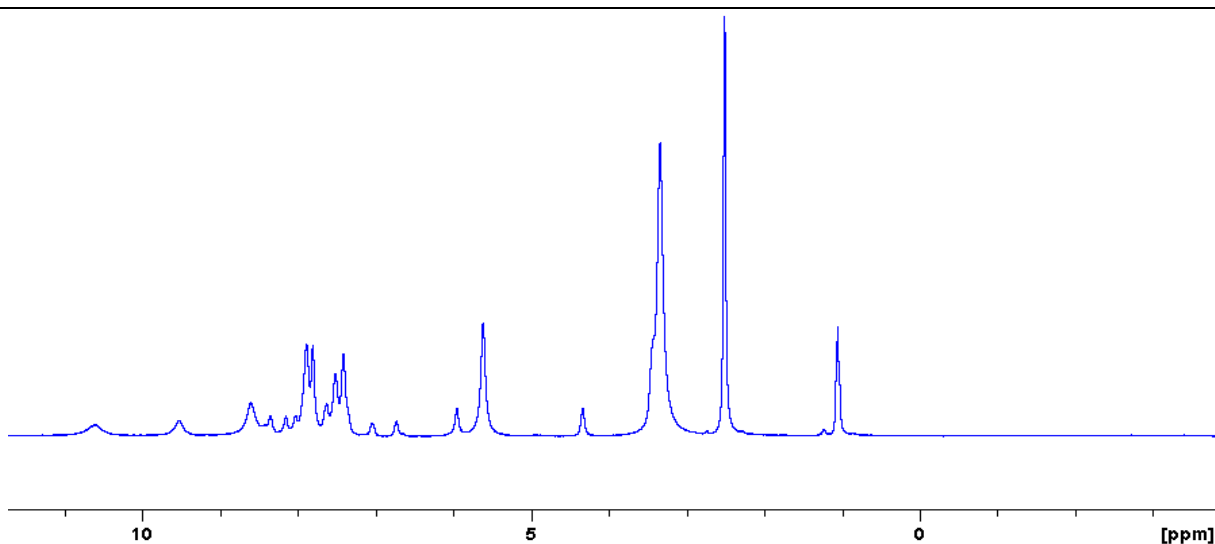
Figure 23: The ^{1}H NMR spectrum for **6** in DMSO-d_6, showing the broad, unresolved signals that are characteristic of paramagnetic complexes.

The structure of **6** revealed that a rare,[44] Cu(II)-NHC complex had formed. The broad, poorly resolved peaks in the ^{1}H NMR (Figure 23), the charge balance in the asymmetric unit (Figure 24), and the presence of Jahn-Teller distortions (see Table 4) support the presence of a Cu(II) complex. Figure 23 shows that the NHC form of **3**, 1,3-bis(pyridin-2-ylmethyl)imidazole-2-ylidene, coordinated to the Cu(II) centre as a tridentate NHC pincer ligand, with a methanol molecule coordinating through its oxygen atom at the fourth equatorial position. The two axial positions are occupied by a SiF_6^{2-} anion and another methanol molecule. The Cu(II)-C bond length in this complex is 1.91452(3) Å, which is on the short end of previously reported Cu(II)-C bond lengths, which range between 1.91 and 2.01 Å.[44-46,61] The bond angles around the copper centre deviate from the ideal octahedral geometry by a similar amount as observed in **5**, which are well within the acceptable range.

Table 4: Selected bond lengths for 6.

Bond	Length/Å	Bond	Length/Å
Cu1-C1	1.91452(3)	Cu1-O1	1.99296(3)
Cu1-N3	2.05734(4)	C1-N1	1.33400(2)
Cu1-N3'	2.08242(4)	C1-N2	1.33704(3)
Cu1-F1	2.56463(6)	Cu1-O2	2.47379(5)

Table 5: Selected bond angles for 6.

Bonds	Angle/°	Bonds	Angle/°
F1-Cu1-O2	171.0445(3)	C1-Cu1-N3	87.8486(16)
C1-Cu1-O1	170.67448(19)	C1-Cu-N3'	89.4130(16)
N3-Cu1-N3'	170.9022(3)	C1-Cu1-O2	86.4836(13)
N1-C1-N2	106.0912(11)	C1-N2-C2	110.4542(5)
C1-N1-C3	110.7441(16)	N1-C3-C2	106.4196(16)
N2-C2-C3	106.2847(11)		
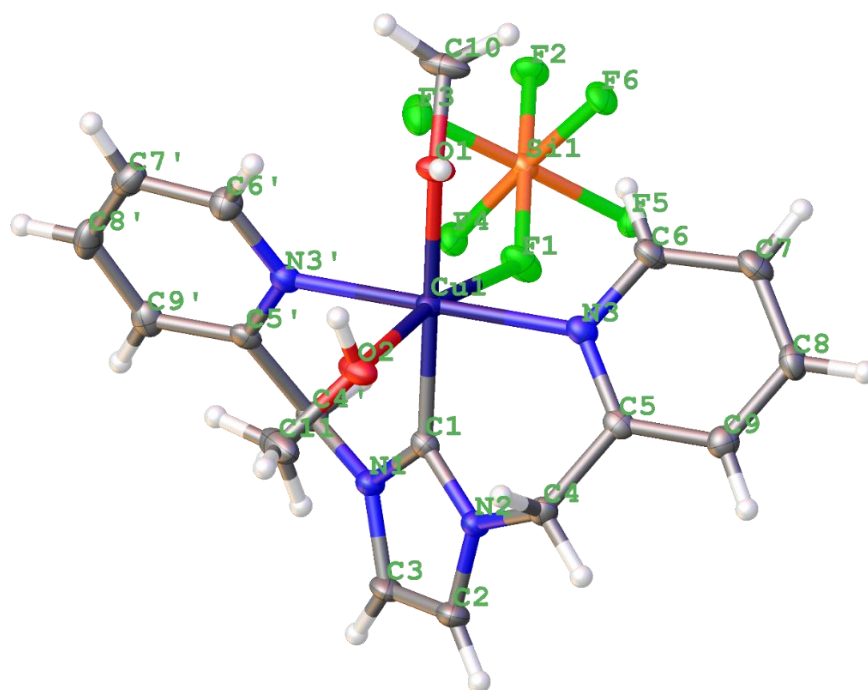
Figure 24: The asymmetric unit of **6**. The thermal ellipsoids are drawn at the 50% probability level.

This structure also contains intermolecular hydrogen bonds between the SIFIX anion and the coordinated methanol molecules. Both interactions are below 2 Å with distances of 1.79738(4) Å for H1-F and 1.92978(3) Å for H2-F4, demonstrating the ability for the SIFSIX anion to form hydrogen bonds. These interactions form 1D hydrogen bonded chains that extend indefinitely through the crystal, running parallel to one another (illustrated in Figure 25). This hydrogen bonding is likely a contributing factor to the stability of **6**.

The SIFSIX anions are held in place as a result of the hydrogen bonding, aiding in crystallization and contributing to the overall stability of the complex. This becomes very evident with the observation of the compact ellipsoids representing the fluorine atoms, which when free, are typically large, and/or disordered due free rotation.
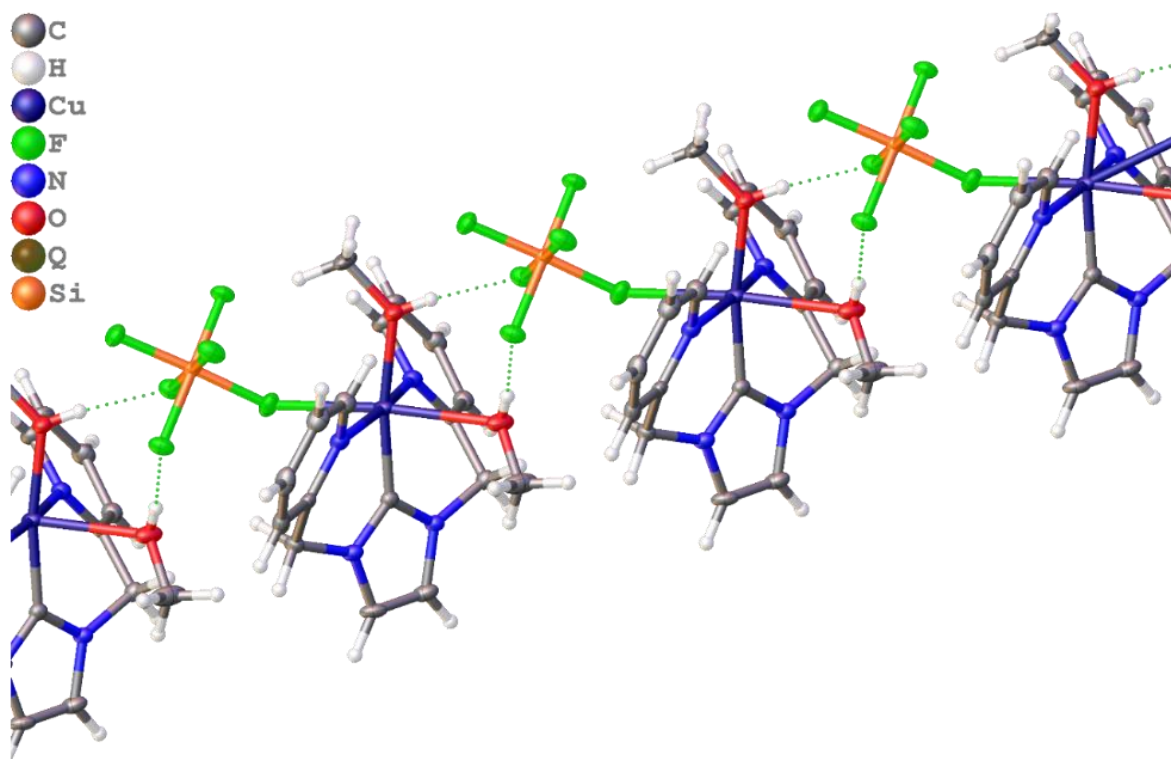
Figure 25: A view of the chains formed by the hydrogen bonds that are present in **6**.

Another factor contributing to the unusual stability of this Cu(II)-NHC complex is the tridentate pincer action of **3**. Although the complex does not contain an anionic tether like many of the other examples,[44-46,61] the presence of coordinating pyridyl or picolyl groups have been shown to stabilize the mismatch in energy levels of the LUMO of Cu(II) and the HOMO of the NHC carbon to some extent.[44] Another stabilizing factor is the presence of the coordinated methanol molecules. Previous reports have shown that oxygen donors stabilize Cu(II)-NHC complexes.[49,62]

Most Cu(II)-NHC complexes that have been reported thus far are synthesized by using NHC transfer reagents, which are typically prepared by reacting the precursor imidazolium salt with Ag_2O to form the bis(NHC)-Ag(I) complex. Once isolated, it is reacted with a Cu(II) salt to form the final complex. This typically requires an inert atmosphere, and dry solvents, making this route inconvenient. There are also examples where the reaction of the free NHC can result in the formation of a Cu(II)-NHC complex. This approach, however, often leads to inconsistent results, and is a difficult route since it involves the isolation of the free NHC ligand.[62] In contrast to these methods, **6** was prepared by direct combination of **3**, and Cu-SIFSIX·H_2O. Remarkably, this took place without heating, exposed to atmospheric moisture, and in methanol that had not been treated with any drying agents. The crystals used for single crystal XRD data collection of **6** were also grown under these conditions, and selected on the lab bench in open air before being placed in Paratone® oil. The data collected was of high quality, making the structure solution straightforward, and indicating high quality crystals. The combination of the simple preparation and moisture tolerance could make this complex applicable for use as a catalyst. Catalysis using similar Cu(II)-NHC complexes was shown to possess improved activity in the Ullmann-type etherification reaction when compared with Cu(I)-NHCs and the bare copper salts.[49] This is likely

attributed to the added stability of the higher oxidation state species that are intermediates in the catalytic cycle.

2.3.3. Preparation and characterization of Bulk Powder Samples of the Coordination Complexes 5-8.

The bulk samples for **5** and **6** were prepared by combining solutions of absolute ethanol containing an equimolar quantity of the respective ligand and the Cu-SIFSIX salt and stirring them overnight.
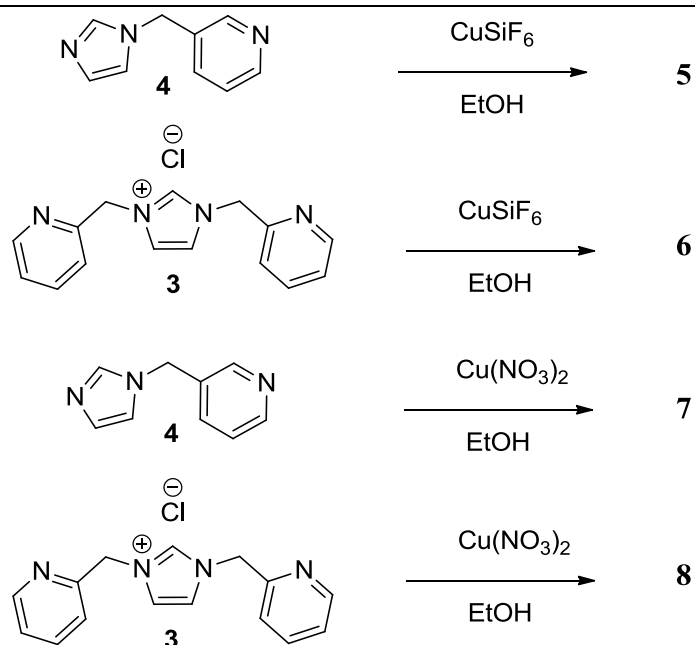
Figure 26: The reaction scheme for the preparation of **5**, **6**, **7**, and **8**.

 The precipitates that formed were then collected by filtration, and the solids were dried in air. The same procedure was carried out for the combination of **4** and Cu(NO₃)₂ (**7**) and the combination of **3** and Cu(NO₃)₂ (**8**). See Figure 26 for an illustration of the reaction scheme.

Attempts to grow single crystals suitable for single crystal XRD analysis have been unsuccessful thus far, but this work is still in progress. The ATR FT-IR spectra of **5-8** were collected, and upon comparison with the starting materials, it is evident that the desired anion and

ligands are present. The tables below (Table 7 and Table 8) summarize the comparison. This comparison shows that the spectral elements from both the ligands and the metal salts used in their synthesis are present in the precipitate that formed. Furthermore, the observed colour change, combined with the formation of a precipitate by the combination of otherwise homogeneous solutions indicates the formation of a complex.

Table 6: The prominent and distinct IR peaks for the starting materials used to synthesize 5 through 8.

$CuSiF_6 \cdot H_2O$ Distinct IR Peaks (cm^{-1})	$Cu(NO_3)_2 \cdot 3H_2O$ Distinct IR Peaks (cm^{-1})	Distinct IR Peaks of **3** (cm^{-1})	Distinct IR Peaks of **4** (cm^{-1})
1666 (m)	1512 (m)	3102 (m)	3082 (m)
1101 (s)	1438 (s)	2946 (s)	2946 (s)
686 (vs)	1322 (vs)	1502 (s)	1564 (s)
	1275 (vs)	1426 (s)	1429 (s)
	757 (s)	734, 706 (vs)	1164 (vs)
			752 (vs)

*The graphical spectra are given in Appendix A.

In both **5** and **6**, the distinct signals from Cu-SIFSIX are expected to be present (Table 6). These are in fact present, as shown in the entries Table 7 denoted ‡ for the columns that are labelled **5** and **6**. In **5**, the presence of the ligand is confirmed by the signal at 3141 cm^{-1} (denoted †). This corresponds to the aromatic C-H stretch of the ligand, which was the only aromatic species added to the reaction mixture. Likewise, **6**, **7**, and **8** all have signals corresponding to the aromatic C-H stretch of the ligands. **7** and **8** should both have signals that arise from $Cu(NO_3)_2$ (shown in Table 6). Both compounds have signals near 1450 and 1275 cm^{-1}, which correspond to the nitrate anion.

Table 7: The prominent and distinct IR peaks for 5, 6, 7, and 8.

Distinct IR Peaks of **5** (cm^{-1})	Distinct IR Peaks of **6** (cm^{-1})	Distinct IR Peaks of **7** (cm^{-1})	Distinct IR Peaks of **8** (cm^{-1})
3141 (m)[†]	3107 (w)[†]	3146 (m)[†]	3138, 3109 (w)[†]
1643 (m)[‡]	2973 (s)[†]	1472 (s)*	1602 (m)[†]
1105 (m)[‡]	1640, 1622 (m)[‡]	1291 (vs)[‡]	1435 (s)[‡]
700 (vs)[‡]	1437 (m)[†]	1101 (s)	1287 (vs)[‡]
	1089, 1047 (s)[‡]		824 (m)
	800-585 (b/vs) split*		769, 762 (s) split*

[‡] Indicates the signal originates from the metal salt. [†] Indicates the signal originates from the ligand. * Indicates the signal originates from a combination of the ligand and metal salt. The graphical spectra are given in Appendix A.

3. Conclusions

The synthesis of a porous coordination polymer was achieved by combining copper-SIFSIX and the neutral ligand *N*-(pyridin-3-ylmethyl)imidazole (**4**), which formed the 1-dimensional CP, **5**. Since SIFSIX coordinated to the axial positions of the copper atoms, **5** demonstrates the ability for SIFSIX to act as a pillar, which would guide the stacking in the formation of a 2D coordination network. **6** also showed this type of arrangement with the SIFSIX anion. Both complexes showed the ability for the SIFSIX anion to form hydrogen bonds as well, which is important in some gas adsorption applications. **6** was found to be a rare, Cu-(II)-NHC complex that was prepared in the presence of atmospheric moisture without the need for NHC transfer reagents. Furthermore, the complex was stable, even though it did not have an anionic tether.

The synthesis of the target ligands was unsuccessful, but many reaction conditions have been ruled out for their preparation. The cause of these unsuccessful attempts was found to be a result of the instability due to self reaction of 3 and 4-(chloromethyl)pyridine that are used in their synthesis. Currently, alternative methods and alternative ligands for this application are being investigated.

4. Future Work

The stability of the Cu(II)-NHC complex (**6**) should be investigated further. **6** should then be tested for reactions in which Cu(I)-NHC ligands are known to be catalysts, in particular, those that are known to involve the formation of higher oxidation state copper species. Furthermore, it would be beneficial to characterize **6** more thoroughly, such as determination of its magnetic susceptibility, and an assessment of the electron density on the copper atom by means of carbonyl ligand IR shift. The gas adsorption characterization of **5** should also be carried out, and the crystal structures for **7** and **8** should be determined, if possible.

A significant portion of the future work should also be focused on the preparation of the proposed ligands, and/or the synthesis of a suitable alternative ligand. Future attempts at preparing **1** and **2** might be successful with the use of a protecting group to block the lone pair of electrons on the nitrogen atom of the pyridine ring. There are several ways in which this can be accomplished. The *N*-oxide can be prepared by simply reacting the freebase in with 3-chlorobenzene-1-carboperoxoic acid (*m*-CPBA) in chloroform at room temperature. Stirring with zinc dust has been successful in removing the *N*-oxide, but results can be variable, especially on large scale reactions.[63] Pyridine *N*-oxides can also be thermally unstable, which could hinder their usefulness.[63] The second method is to use BH_3 as a protecting group, which has been done for a substrate suffering from a similar problem as 3 and 4-(chloromethyl)pyridine.[63] An example from the literature is shown in Figure 27.
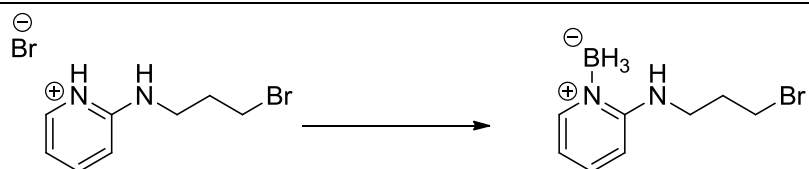
Figure 27: The substrate that was protected in the literature.[63]
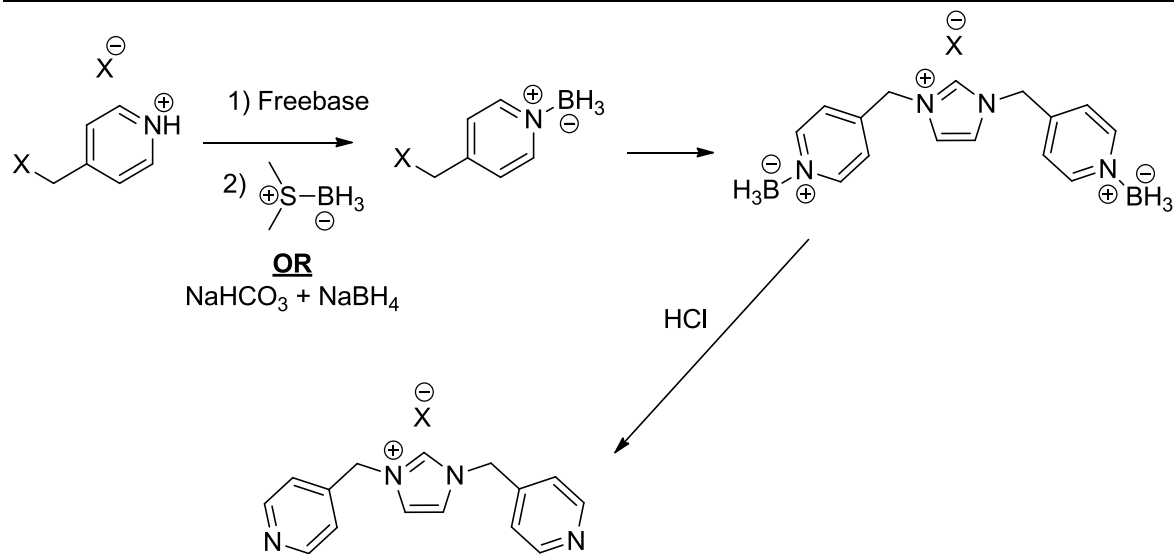
Figure 28: The suggested protection, deprotection scheme for the synthesis of the proposed ligands.

Once protected, the intermediate from the literature is stable in refluxing acetonitrile, and in the presence of potassium carbonate, and would not undergo the undesirable cyclization.[63] In the scheme shown in Figure 28, there are several ways to achieve the first step of the reaction. The first of the two listed is specific to the reaction shown in Figure 27,[63] and the second method listed has been used to prepare a wide range of amine-borane complexes, and does not require the use of anhydrous conditons.[64] This method, being more general and tolerant to moisture should be the preferred route with which to proceed.

5. Experimental

5.1. Materials and General Considerations

All chemicals were purchased from Sigma Aldrich, Alfa Aeser, Oakwood Chemicals, Fisher Scientific, Caledon Laboratories, and were used without further purification. Deuterated NMR solvents were purchased from Cambridge Isotopes, or Sigma Aldrich. A Bruker 300 MHz Ultrashield spectrometer was used to obtain all NMR spectra. IR spectra were obtained using a Bruker ALPHA Platinum ATR fitted with a single reflection diamond. ESI-MS data were obtained using the Agilent 1100 LC/MSD Trap. All single crystal X-ray diffraction data were collected using a Bruker Apex-II CCD diffractometer using a MoKα (λ = 0.71073) radiation source. Data was integrated using Bruker ApexII. Structure solutions were obtained with SHELXT using the intrinsic phasing method and structure refinement was carried out using SHELXL using least squares method, both interfaced with Olex^2.[65-67]

5.2. Procedures for the Attempted Synthesis of 1 and 2

Entry 1 (Table 1)

3-(Bromomethyl)pyridine hydrobromide (2.10 mmol/0.531 g) was dissolved in 10 mL of water. The solution was transferred to a separatory funnel along with 10 mL of dichloromethane. Dropwise, with frequent shaking, a saturated solution of sodium carbonate was added until the aqueous layer was basic by pH paper. The organic fraction was collected, and the aqueous layer was extracted with dichloromethane (2x25 mL). The organic fractions were combined, dried over anhydrous magnesium sulfate, and filtered by gravity. This solution was added slowly *via* a dropping funnel, over 15 minute period, to a 100 mL round bottom flask containing dichloromethane (5 mL), *N*-(trimethylsilyl)imidazole (1.0 mmol/0.13 mL) and a magnetic stir bar. The solution was stirred for 22 hours at room temperature.

Entry 2 (Table 1)

In a 250 mL round bottom flask, imidazole (1.00 mmol/0.068 g), 3-(bromomethyl)pyridine hydrobromide (2.00 mmol/0.506 g), sodium carbonate (4.00 mmol/0.424 g), and acetonitrile (160 mL) were combined along with a magnetic stir bar. The mixture was held under reflux for 18 hours. After cooling, the mixture was filtered by gravity, then the solvent removed by rotary evaporation at 68 °C, which afforded a reddish-brown solid. This was taken up in dichloromethane and added dropwise to 200 mL of ice cold diethyl ether with rapid stirring. The ether was decanted off the resulting solid, which was washed further with diethyl ether. The solid was then dried in *vacuo*.

Entry 3 (Table 1)

In a 250 mL round bottom flask, imidazole (1.00 mmol/0.068 g), 4-(bromomethyl)pyridine hydrobromide (2.00 mmol/0.506 g), sodium carbonate (4.00 mmol/0.424 g), and acetonitrile (160 mL) were combined along with a magnetic stir bar. The mixture was held under reflux for 18 hours. The solvent was then removed by rotary evaporation at 48 °C, and the resulting solid was extracted with methanol, leaving behind an off white solid. The methanol was removed, then the resulting solid was dissolved in a minimal amount of methanol and dropped into ice cold diethyl ether, resulting in the formation of a precipitate. The ether was decanted, and the solid was washed further with ether, then dried in *vacuo*.

Entry 4 and 5 (Table 1)

In a 250 mL round bottom flask, imidazole (18.05 mmol/1.23 g), 4-(chloromethyl)pyridine hydrochloride (entry 4) or 4-(chloromethyl)pyridine hydrochloride (entry 5) (36.1 mmol/5.93 g), sodium bicarbonate (56.0 mmol/4.56 g), and anhydrous ethanol (50 mL) were combined along with a magnetic stir bar. The mixture was held under reflux for 48 hours, then filtered by gravity

after cooling. The solvent was then removed by rotary evaporation, resulting in a residue. This was extracted with dichloromethane by stirring overnight, after which time, there was still material that remained undissolved. The dichloromethane was removed by rotary evaporation, resulting in a dark brown oil. This was triturated with the addition of tetrahydrofuran, resulting in a dark brown powder. After the solvent was decanted, the powder was washed twice more with tetrahydrofuran. The ^{1}H NMR spectrum at this point indicated the substance was very impure, so the solid was then taken up in a minimal amount of methanol and dropped into diethyl ether with stirring. The solvent was decanted, and the resulting solid was washed twice more with diethyl ether. After drying in *vacuo*, the ^{1}H NMR still indicated poor purity, so 200 mL of dry acetonitrile was added and heated to 80 °C with stirring. The solution was decanting. This process was repeated (120 mL of acetonitrile), which resulted in a supernatant that was much lighter in colour. The remaining solid was washed with smaller portions of acetonitrile until the washes were no longer coloured. This solid was then dissolved in water, extracted with diethyl ether (3x25 mL), and the aqueous layer was evaporated, and the solid dried in *vacuo*.

Entry 6 and 7 (Table 1)

4-(chloromethyl)pyridine hydrochloride (entry 5) or 3-(chloromethyl)pyridine hydrochloride (entry 6) (6 mmol/2.03 g) was dissolved in *ca.* 60 mL of water. Saturated sodium hydroxide was slowly added until the solution was basic by pH paper, then it was extracted with diethyl ether (3x20 mL). The ether fractions were combined, dried with anhydrous magnesium sulfate and filtered by gravity. To this, *N,N*-dimethylformamide was added (10 mL) and the ether was removed in *vacuo*. The solution was transferred to a dry, 35 mL microwave tube containing imidazole (6.00 mmol/0.408 g) and a stir bar. 95% sodium hydride (6.10 mmol/0.154 g) was cautiously added, and after the foaming was settled down, the cover was placed on the tube, and

the tube was placed in the microwave reactor, which was set with the following parameters. T = 110 °C, power = 100 W, pressure = 3.5 bar, stirring = high, time = 2-4 hours, mode = dynamic. After the time was complete, the solution was added to a 250 mL round bottom flask. Diethyl ether was added to this which precipitated a brown, goopy substance. Attempts to recrystallize this from methanol by diffusion of diethyl ether were unsuccessful at removing the impurities.

Entry 8 and 9 (Table 1)

4-(chloromethyl)pyridine hydrochloride (entry 8) or 3-(chloromethyl)pyridine hydrochloride (entry 9) (6 mmol/2.03 g) was dissolved in *c.a.* 60 mL of water. Saturated sodium hydroxide was slowly added until the solution was basic by pH paper, then it was extracted with diethyl ether (3x20 mL). The ether fractions were combined, dried with anhydrous magnesium sulfate and filtered by gravity. To this, acetonitrile was added (10 mL) and the ether was removed in *vacuo*. The solution was transferred to a dry, 35 mL microwave tube containing imidazole (6.00 mmol/0.408 g) and a stir bar. 95% sodium hydride (6.10 mmol/0.154 g) was cautiously added, and after the foaming was settled down, the cover was placed on the tube, and the tube was placed in the microwave reactor, which was set with the following parameters. T = 80 °C, power = 100 W, pressure = 3.5 bar, stirring = high, time = 2-4 hours, mode = dynamic. After the time was complete, the solution was added to a 250 mL round bottom flask. Diethyl ether was added to this which precipitated a brown, goopy substance. Attempts to recrystallize this from methanol by diffusion of diethyl ether were unsuccessful.

Entry 11 (Table 1)

In a 50 mL Schlenk flask under an atmosphere, imidazole (1.0 mmol/0.068 g) was dissolved in 4 mL of anhydrous tetrahydrofuran. With stirring, 95% sodium hydride (1.1 mmol/0.028 g) was cautiously added. The suspension was stirred for 30 minutes. While stirring,

4-(chloromethyl)pyridine hydrochloride (2.1 mmol/0.352 g) was dissolved in water and the freebase was generated by adding saturated sodium hydroxide until the solution was basic by pH paper. The freebase was extracted with diethyl ether (3x5 mL), dried with anhydrous magnesium sulfate, and then filtered by gravity. Tetrahydrofuran (5 mL) was added to this and most of the diethyl ether was removed in *vacuo*. Using a cannula, the solution containing the freebase was transferred to a dropping funnel and slowly added to the Schlenk flask. After the addition, a vacuum was drawn on the system to reduce the volume of the reaction solvent. After stirring overnight, the solvent was decanted leaving behind a red solid, which was washed with diethyl ether.

Entry 12 (Table 1)

In 50 mL round bottom flask equipped with a magnetic stir bar, 4-(aminomethyl)pyridine (98%) (5.00 mmol/0.518 mL) and toluene (5 mL) were combined. With vigorous stirring, paraformaldehyde (5.00 mmol/0.150 g) was added. After 30 minutes, there was a clear crystalline precipitate present. The mixture was cooled to 0 °C, then another equivalent of 4-(aminomethyl)pyridine (98%) (5.00 mmol/0.518 mL) was added. After 10 minutes at 0 °C, aqueous tetrafluoroboric acid (48%) (6.25 mmol/0.815 mL) was added slowly over a 15 minute period of time, which afforded a sticky white precipitate. The mixture was warmed to room temperature, then aqueous glyoxal (40%) (5.00 mmol/0.574 mL) was slowly added. As the addition took place, the mixture took on an orange colour that intensified with time. The mixture was heated to 50 °C and stirred overnight. The result was a mixture that was a red/brown colour, including a sticky, non-soluble solid after it had cooled. Dichloromethane (10 mL) and water (5 mL) were added and the mixture was poured into a separatory funnel. The organic layer was collected, then the aqueous layer was extracted with dichloromethane (2x10 mL). The fractions

were combined, dried with magnesium sulfate, filtered, then the solvent was removed by rotary evaporation. The [1]NMR spectrum of the resulting residue revealed a mixture that did not include what is expected for the desired product. The residual goopy solid that was left in reaction flask was extracted with methanol. The volume was reduced, then a red crystalline powder was precipitated upon the addition of diethyl either. The ^{1}H NMR spectrum revealed that this was not the desired product either.

5.3. Synthesis of Successfully Isolated Compounds (3-8)

Synthesis of 1,3-bis(pyridin-2-ylmethyl)imidazolium chloride (3)

1,3-bis(pyridin-2-ylmethyl)imidazolium chloride was prepared using a modified method from the literature.[38,52]

Imidazole (99%) (5.00 mmol/0.340 g), 2-(chloromethyl)pyridine hydrochloride (97%) (10.00 mmol/ 1.66 g) and sodium bicarbonate (15.10 mmol/1.30 g) were taken up in anhydrous ethanol (15 mL). The mixture was held under reflux for 48 hours with stirring, then allowed to cool to room temperature. It was then filtered by gravity, and the solvent was removed by rotary evaporation. The brown residue was then taken up in dichloromethane, dried with anhydrous magnesium sulfate, and filtered by gravity. The solvent was again removed. Tetrahydrofuran was added (*c.a.* 15 mL) and a small amount of dichloromethane (2-4 mL), and the mixture was swirled, which resulted in a brown powder to precipitate. The solvent was decanted, and the solid was washed with tetrahydrofuran (2x5 mL) and dried in *vacuo*. Yield: 0.818 g/2.86 mmol/57% ^{1}H NMR (CDCl$_3$, 300 MHz) δ (ppm) 10.85 (s, 1H), 8.53-8.51 (m, 2H), 7.75-7.71 (m, 4H), 7.68-7.67 (m, 2H), 7.31-7.23 (m, 2H), 5.72 (s, 4H). ^{13}C NMR (CDCl$_3$, 300 MHz) δ (ppm) 152.53, 149.86, 137.59, 137.68, 124.01, 123.91, 122.49, 54.13. FT- IR (ATR, cm^{-1}) 3082 (m), 2945 (s), 1893 (w),

1800 (w), 1666 (w), 1564 (s), 1429 (s), 1164 (vs), 752 (vs). ESI-MS (+): Calcd for $C_{15}H_{15}N_4$ m/z: 251.13. Found m/z: 251.1.

Isolation of *N*-(pyridin-3-ylmethyl)imidazole (4) as a By-product

After the reaction of entry 5 in Table 1 had taken place, the crude mixture was filtered by gravity. The solvent was removed, and the residue was extracted with several portions of dichloromethane. The after removal of the dichloromethane, the resulting residue was washed with several portions of tetrahydrofuran (THF). The THF was removed under reduced pressure to give **2** as a yellow oil, which eventually crystallized after drying in *vacuo*. ^{1}H NMR (CDCl$_3$, 300 MHz) δ (ppm) 8.51-8.50 (m, 1H), 8.44-8.43 (m, 1H), 7.50 (s, 1H), 7.39-7.35 (m, 1H), 7.24-7.20 (m, 1H), 7.02 (1H, s), 6.85-6.84 (1H, m), 5.09 (2H, s). ^{13}C NMR (CDCl$_3$, 300 MHz) δ (ppm) 149.55, 148.46, 137.14, 134.73, 131.75, 129.94, 123.67, 118.98, 48.03. FT- IR (ATR, cm^{-1}): 3102 (m), 1581 (m), 1502 (s), 1426 (s), 808 (s), 734 (vs), 706 (vs).

Synthesis of {Cu(II)[(OH$_2$)$_2$(*N*-(pyridin-3-ylmethyl)imidazole)$_2$]-Cu(II)[(SiF$_6$$^{2-}$)$_2$(*N*-(pyridin-3-ylmethyl)imidazole)]}$_n$ (5)

N-(pyridin-3-ylmethyl)imidazole (0.35 mmol/56 mg) was dissolved in 2 mL of anhydrous ethanol. Separately, copper(II)hexafluorosilicate hydrate (0.35 mmol/72 mg) was dissolved in 6 mL of anhydrous ethanol. These two solution were combined and stirred at room temperature overnight. The resulting blue powder precipitate was isolated by filtration, and washed with several portions of ethanol (air dried yield: 84 mg). This solid was dissolved in water, and after acetone diffused into it for 1-2 weeks, crystals suitable for single crystal X-ray diffraction were collected.

Synthesis of Cu(1,3-bis(pyridin-2-ylmethyl)imidazolylidene)(MeOH)$_2$(SiF$_6$$^{2-}$) (6)

1,3-bis(pyridin-2-ylmethyl)imidazolium chloride (0.15 mmol/43 mg) was dissolved in methanol (2 mL) and added to a solution of copper(II)hexafluorosilicate hydrate (0.15 mmol/31

mg) in methanol (4 mL) in a vial equipped with a magnetic stir bar. As the stirring proceeded, the solution took on a green colour that intensified with time. This green colour was overtaken by blue, and the solution stirred overnight. After 17 hours, an electric blue precipitate had formed. The supernatant (green) was removed, and the electric blue solid was washed with methanol. The solid was found to be slightly soluble in methanol, and vapour diffusion of chloroform into the methanol solution for several days resulted in block shape crystals suitable for single crystal X-ray diffraction.

Synthesis of 5 Bulk

N-(pyridin-2-ylmethyl)imidazolium chloride (0.35 mmol/100 mg) was dissolved in 2 mL of anhydrous ethanol. Separately, copper(II)hexafluorosilicate hydrate (0.35 mmol/72 mg) was dissolved in 6 mL of anhydrous ethanol. These two solution were combined and stirred at room temperature overnight. The resulting blue powder precipitate was isolated by filtration, and washed with several portions of ethanol (air dried yield: 235.4 mg).

Synthesis of 6 Bulk

1,3-bis(pyridin-2-ylmethyl)imidazolium chloride (0.35 mmol/100 mg) was dissolved in 2 mL of anhydrous ethanol. Separately, copper(II)hexafluorosilicate hydrate (0.35 mmol/72 mg) was dissolved in 6 mL of anhydrous ethanol. These two solution were combined and stirred at room temperature overnight. The resulting blue powder precipitate was isolated by filtration, and washed with several portions of ethanol (air dried yield: 235.4 mg).

Synthesis of 7

1,3-bis(pyridin-2-ylmethyl)imidazolium chloride (0.35 mmol/100 mg) was dissolved in 2 mL of anhydrous ethanol. Separately, copper(II)nitrate trihydrate (0.35 mmol/85 mg) was dissolved in 6 mL of anhydrous ethanol. These two solution were combined and stirred at room

temperature overnight. The resulting blue powder precipitate was isolated by filtration, and washed with several portions of ethanol (air dried yield: 44.3 mg).

Synthesis of 8

N-(pyridin-3-ylmethyl)imidazole (0.35 mmol/56 mg) was dissolved in 2 mL of anhydrous ethanol. Separately copper(II)nitrate trihydrate (0.35 mmol/85 mg) was dissolved in 6 mL of anhydrous ethanol. These two solution were combined and stirred at room temperature overnight. The resulting blue powder precipitate was isolated by filtration, and washed with several portions of ethanol (air dried yield: 110.9 mg).

6. References

1. Batten, S. R.; Champness, N. R.; Chen, X. M.; Garcia-Martinez, G.; Kitagawa, S.; Öhrström, L.; O'Keeffe, M.; Suhh, M. P.; Reedijk, J. *Cryst. Eng. Comm.* **2012**, *14*, 3001-3004.

2. Horike, S; Kitagawa, S .Design of Porous Coordination Polymers/Metal-Organic Frameworks: Past, Present and Future. In *Metal-Organic Frameworks: Applications from Catalysis to Gas Storage*; Farrusseng, D., Eds.; Wiley-VCH Verlag: Weinheim, Germany, 2011, pp 3-21.

3. Nugent, P.; Belmabkhout, Y.; Burd, S. D.; Cairns, A. J.; Luebke, R.; Forrest, K.; Pham, T.; Ma, S.; Space, B.; Wojtas, L.; Eddaoudi, M.; Zaworotko, M. J. *Nature*. **2013**, *495*, 80-85.

4. Cui1, X.; Chen, K.; Xing, H.; Yang, Q.; Krishna, R.; Bao1, Z.; Wu, H.; Zhou, W.; Dong, X.; Han, Y.; Li, B.; Ren, Q.; Zaworotko, M. J.; Chen, B. *Science*. **2016**, *353(6295)* 141-144.

5. Leroux, M.; Mercier, N.; Allain, M.; Dul, M. C.; Dittmer, J.; Kassiba, A. H.; Bellat, J. P.; Weber, G.; Bezverkhyy, I. *Inorg. Chem.* **2016**, *55*, 8587-8594.

6. Kong, G. Q.; Ou, S.; Zou, C.; Wu, C. C. *J. Am. Chem. Soc.* **2012**, *134*, 19851-19857.

7. Karmakar, A; Desai, A. V.; Ghosh, S. K. *Coord. Chem. Rev.* **2016**, *307*, 313-341.

8. Desai, A. V.; Manna, B.; Karmakar, A.; Sahu, A.; Ghosh, S. K. *Angew. Chem. Int. Ed*. **2016**, *55*, 7811-7815.

9. Shibata, Y. *J. Coll. Sci. Imp. Univ. Tokyo.* **1916**, *37*, 1-31.

10. Keggin, J. F.; Miles, F. D.; *Nature*. **1936**, *137*, 577-578.

11. Iwamoto, T.; Miyoshi, T.; Miyamoto, T.; Sasaki, Y.; Fujiwara, S. *Bull. Chem. Soc. Jpn*. **1967**, *40*, 1174-1178.

12. Powell, H. M.; Rayner, J. H. *Nature*. **1949**, *163*, 566-567.

13. Kinoshita, Y.; Matsubara, I.; Higuchi, T.; Saito, Y. *Bull. Chem. Soc. Jpn*. **1959**, *32*, 1221-1226.

14. Yaghi, O. M.; Li, G.; Li, H. *Nature*. **1995**, *378*, 703-706.

15. Jin, K.; Huang, X.; Pang, L.; Li, J.; Appelb, A.; Wherland, S. *Chem. Commun*. **2002**, *23* 2872-2873.

16. Kondo, M.; Okubo, T.; Asami, A.; Noro, S.; Yoshitomi, T.; Kitagawa, S.; Ishii, T.; Matsuzaka, H.; Seki, K. *Angew. Chem. Int. Ed.* **1999**, *38(1/2)*, 140-143.

17. Janiak, C. *Dalton Trans*. **2003**, *14*, 2781-2804.

18. JeongYong Lee, J. Y.; Omar K. Farha, O. K.; John Roberts, J.; Karl A. Scheidt, K. A.; SonBinh T. Nguyen S. B. T.; and Joseph T. Hupp, J. T. *Chem. Soc. Rev*. **2009**, *38*, 1450-1459.

19. Chughtai, A. H.; Ahmad, N.; Younus, H. A.; Laypkovc, A.; Verpoort, F. *Chem. Soc. Rev*. **2015**, *44*, 6804-6849.

20. Chen, D. M.; Tian, J. Y.; Liu, C. S.; Chen, M.; Du, M. *Chem. Eur. J.* **2016**, *22*, 15035-15041.

21. Leroux, M.; Mercier, N.; Allain, M.; Dul, M. C.; Dittmer, J.; Kassiba, A. H.; Bellat, J. P.; Weber, G.; Bezverkhyy, I. *Inorg. Chem.* **2016**, *55*, 8587-8594.

22. Kong, G. Q.; Ou, S.; Zou, C.; Wu, C. C. *J. Am. Chem. Soc.* **2012**, *134*, 19851-19857.

23. Hao, X. L.; Ma, Y. Y.; Zang, H. Y.; Wang, Y. H.; Li, Y. H.; Wang, E. B. A. *Chem. Eur. J*. **2015**, *21*, 3778-3784.

24. Shu, M.; Tu, C.; Xu, W.; Jin, H.; Sun, J. *Cryst. Growth Des*. **2006**, *6(8)*, 1890-1896.

25. Desai, A. V.; Manna, B.; Karmakar, A.; Sahu, A.; Ghosh, S. K. *Angew. Chem. Int. Ed*. **2016**, *55*, 7811-7815.

26. Seo, J. S.; Whang, D.; Lee, H.; Jun, S. I.; Oh, J.; Jeon, Y. J.; Kim, K. *Nature*. **2000**, *404*, 982-986.

27. Mao, C.; Kudla, R. A.; Zuo, F.; Zhao, X.; Mueller, L. J.; Bu, X.; Feng, P.; *J. Am. Chem. Soc.* **2014**, 136, 7579-7582.

28. Suresh, E.; Bhadbhade, M. M. *Cryst. Eng. Comm*. **2001**, *13*, 1-3.

29. Wang, X.; Lin, H.; Bi, Y.; Chen, B.; Liu, G. *J. Solid State Chem*. **2008**, *181*, 556-561.

30. Wang, X.; Hu, H.; Chen, B.; Lin, H.; Tian, A.; Li, J. *Solid State Sci.* **2011**, *13*, 344-349.

31. Qi, X. L.; Lin, R. B.; Chen, Q.; Lin, J. B.; Zhang, J. P.; Chen, X. M. *Chem. Sci.* **2011**, *2*, 2214-2218.

32. Yi, F. Y.; Li, J. P.; Wu, D.; Sun, Z. M. *Chem. Eur. J*. **2015**, *21*, 11475-11482.

33. Nelson, D. J.; Nolan, S. P. *N*-Heterocyclic Carbenes. In *N-Heterocyclic Carbenes: Effective Tools for Organometallic Synthesis*; Nolan, S. P., Eds.; Wiley-VCH Verlag: Weinheim, Germany, 2014, pp 1-24.

34. Wanzlick, H. W. *Angew. Chem. Int. Ed*. **1962**, *1*, 75-80.

35. Wanzlick, H. W.; Schröner, H. L. *Angew. Chem. Int. Ed*. **1968**, *7*, 141-142.

36. Arduengo, A. J.; Harlow, R. L.; Kline, M. *J. Am. Chem. Soc.* **1991**, *113*, 5530-5534.

37. Itoh, T.; Nakata, Y.; Hirai, K.; Tomioka, H. *J. Am. Chem. Soc.* **2005**, *128*, 957-967.

38. Tulloch, A. A. D.; Danopoulos, A. A.; Kleinhenz, S.; Light, M. E.; Hursthouse, M. B.; Eastham, G. *Organometallics*. **2001**, *20*, 2027-2031.

39. Nemcsok, D.; Wichmann, K.; Frenking, G. *Organometallics*. **2004**, *23*, 3640-3646.

40. Vougioukalakis, G. C.; Grubbs, R. H. *Chem. Soc. Rev.* **2009**, *110*, 1746-1787.

41. Díez-González, S.; Nolan, S. P. *Coord. Chem. Rev.* **2007**, *251*, 874-883.

42. Magill, A. M.; McGuinness, D. S.; Cavell, K. J.; Britovsek, G. J. P.; Gibson, V. C.; White, A. J. P.; Williams, D. J.; White, A. H.; Skelton, B. W. *J. Organomet. Chem.* **2001**, *617-618*, 546-560.

43. Egbert, J. D.; Cazin, C. S. J.; Nolan, S. P. *Catal. Sci. Technol.* **2013**, *3*, 912-926.

44. Lake, B. R. M.; Willans, C. E. *Organometallics*. **2014**, *33*, 2027-2038.

45. Arnold, P. L.; Rodden, M.; Davis, K. M.; Scarisbrick, A. C.; Blake, A. J.; Wilson, C. *Chem. Commun.* **2004**, *14*, 1612-1613.

46. Van Veldhuizen, J. J.; Campbell, J. E.; Giudici, R. E.; Hoveyda, A. H. *J. Am. Chem. Soc.* **2005**, *127*, 6877-6882.

47. Jürgens, E.; O.; Mayer, J. J.; Heinze, K.; Kunz, D. *Zeitschrift für Naturforschung B. 71(10)*, 1011-1018.

48. Mao, J. X.; Steckel, J. A.; Yan, F.; Dhumal, N.; Kimc, H.; Damodaran, K. *Phys. Chem. Chem. Phys.* **2016**, *18*, 1911-1917.

49. North, M.; Pasquale, R.; Young, C. *Green Chem.* **2010**, *12*, 1514-1539.

50. Wang, J.; Sng, W.; Yi, G.; Zhang, Y. *Chem. Commun.* **2015**, *51*, 12076-12079.

51. Xie, Y.; Zhang, Z.; Jiang, T. He, J.; Han, B.; Wu, T.; Ding, K. *Angew. Chem. Int. Ed.* **2007**, *46*, 7255-7258.

52. Zhanga, Z.; Yanga, Y.; Suna, H.; Cao, R. *Inorganica Chimica Acta*. **2015**, *434*, 158-171.

53. Ziaee, A.; Chovan, D.; Lusi, M.; PerryIV, J. J.; Zaworotko, M. J.; Tofail, S. A. M. *Cryst. Growth Des.* **2016**, *16*, 3890-3897.

54. Chapman, M. R.; Lake, B. R. M.; Pask, C. M.; Nguyen, B. N.; Willans, C. E. *Dalton Trans*. **2015**, *44*, 15938-15948.

55. Siraj, I. T.; Spicer, M. D. *Int. J Chem. Eng. Appl*. **2013**, *4(4)*, 199-203.

56. Spectral Database for Organic Compounds SDBS, dimethylamine hydrochloride, < http://sdbs.db.aist.go.jp/sdbs/cgi-bin/direct_frame_disp.cgi?sdbsno=2758 > (accessed March 19, 2017).

57. Hesek, D.; Lee, M.; Noll, B. C.; Fisher, J. F.; Mobashery, S. *J. Org. Chem*. **2009**, *74*, 2567-2570.

58. Hans, M.; Lorkowski1, J.; Demonceau, A.; Delaude, L. Beilstein *J. Org. Chem*. **2015**, *11*, 2318-2325.

59. Wouters, J.; Demonceau, A.; Delaude, L. *Chem. Eur. J*. **2015**, *21*,10870-10877.

60. Halcrow, M. A. *Chem. Soc. Rev*. **2013**, *42*, 1784-1795.

61. Larsen, A. O.; Leu, W.; Oberhuber, C. N.; Campbell, J. E.; Hoveyda, A. H. *J. Am. Chem. Soc.* **2004**, *126*, 11130-11131.

62. Kolychev, E. L.; Shuntikov, V. V.; Khrustalev, V. N.; Bush, A. A.; Nechaev, M. S. *Dalton Trans*. **2011**, *40*, 3074-3076.

63. Zajac, M. A. *J. Org. Chem*. **2008**, *73*, 6899-6901.

64. Ramachandran, P. V.; Kulkarni, A. S.; Zhao, Y.; Jianguo Mei, *J. Chem. Commun*. **2016**, *52*, 11885-11888.

65. Sheldrick, G.M. *Acta Cryst*. **2015**, *C71*, 3-8.

66. Burla, M. C.; Caliandro, R.; Camalli, M.; Carrozzini, B.; Cascarano, G. L.; De Caro, L.; Giacovazzo, C.; Polidori, G.; Siliqi, D.; Spagna, R. *J. Appl. Cryst*. **2007**, *40*, 609-613.

67. Dolomanov, O.V.; Bourhis, L.J.; Gildea, R.J.; Howard, J.A.K.; Puschmann, H., OLEX2: A complete structure solution, refinement and analysis program. *J. Appl. Cryst*. **2009,** *42*, 339-341.

7. Appendix

7.1. Appendix A: Spectra for Synthesized Compounds and Select Starting Materials
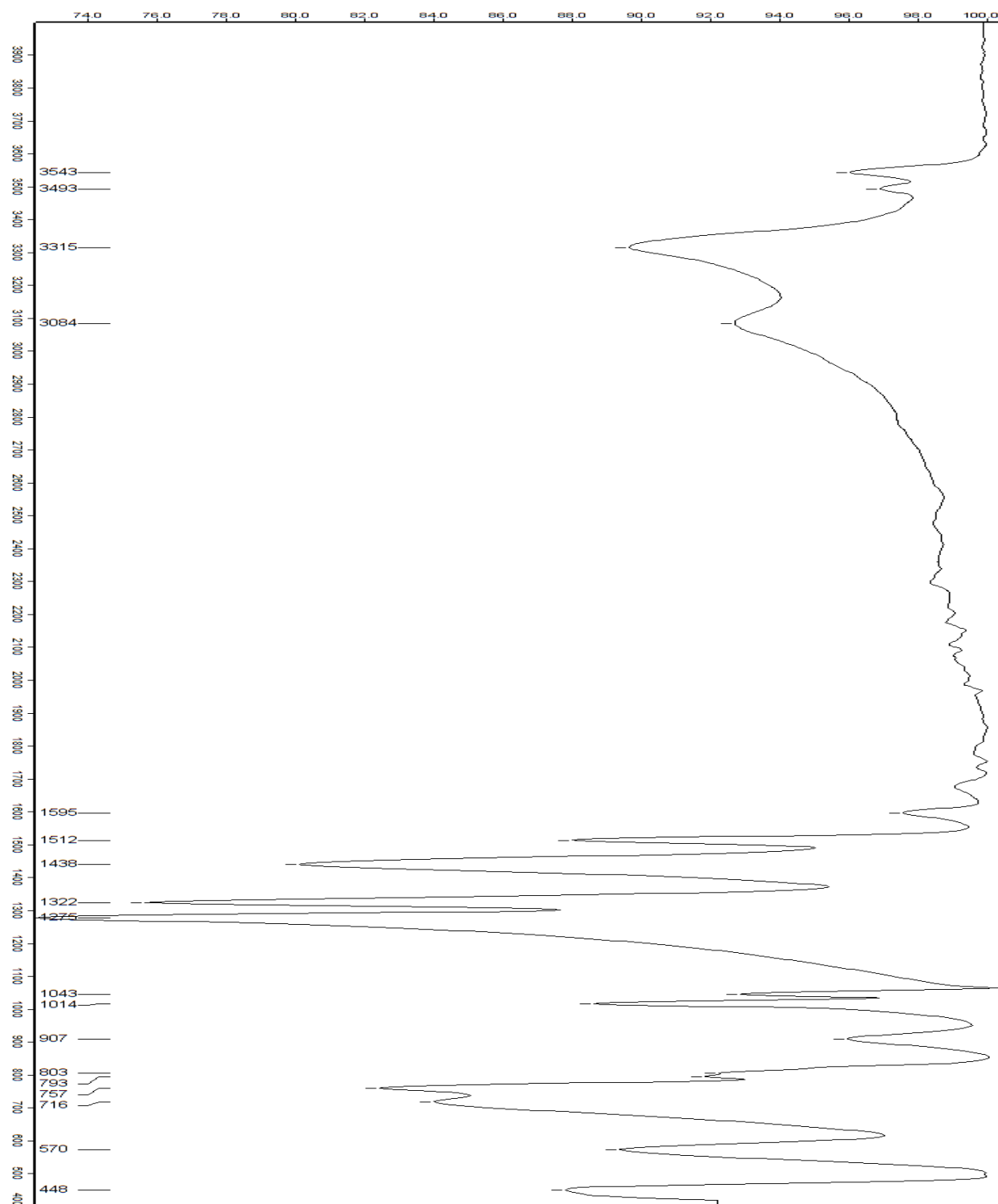
IR spectrum of Cu(NO₃)·H₂O
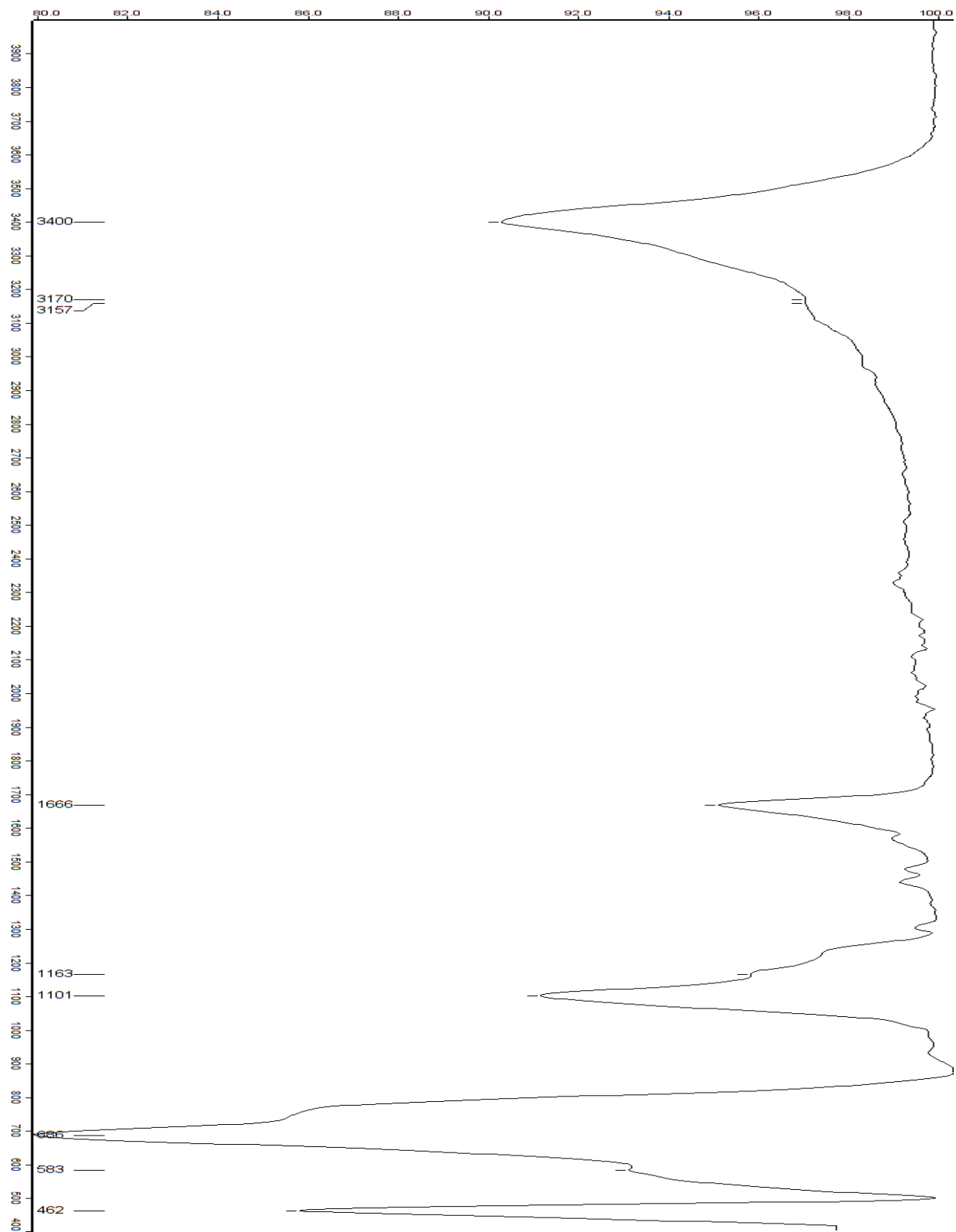
IR Spectrum of CuSiF$_6$·H$_2$O
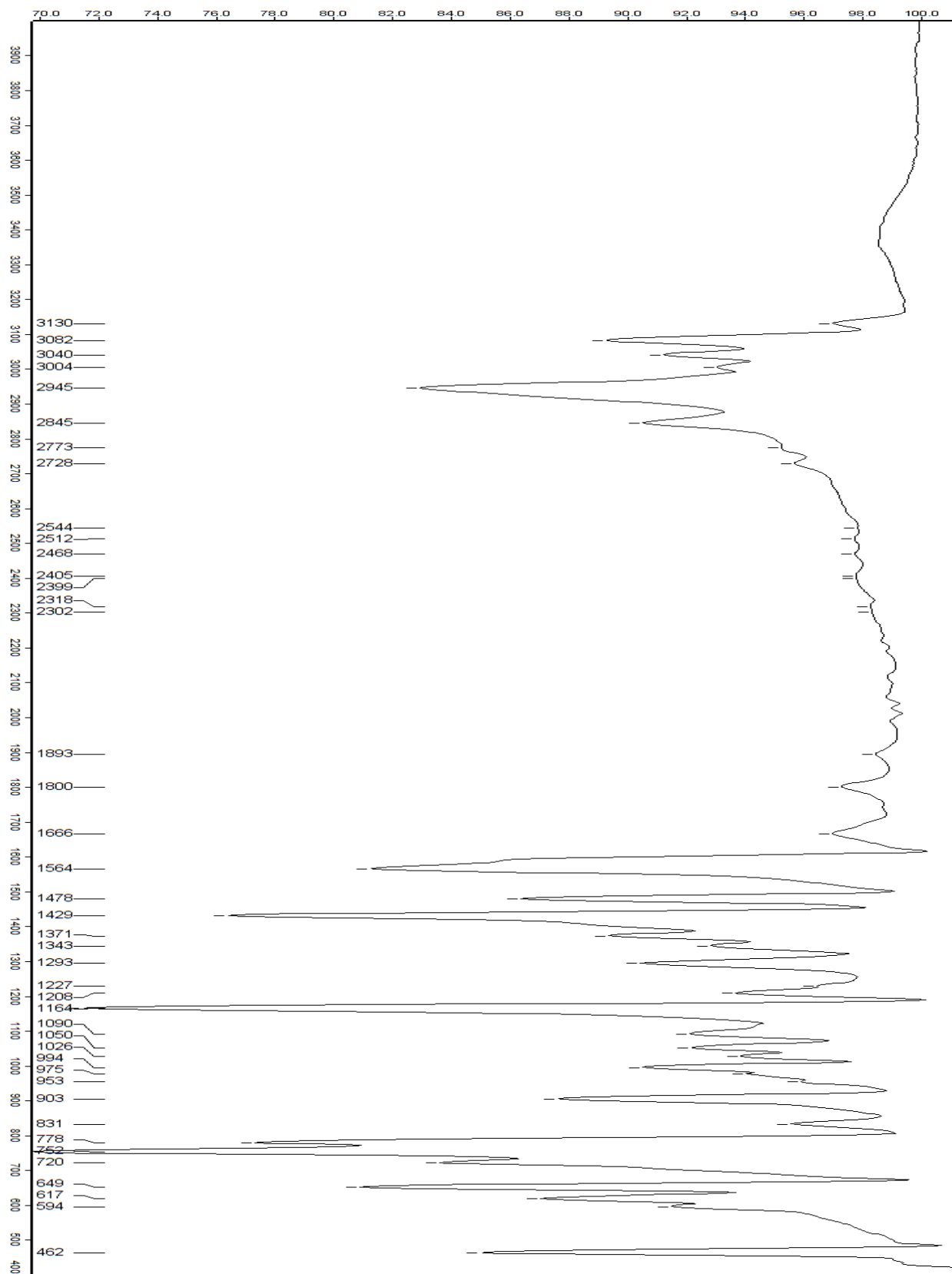
IR Spectrum of 3
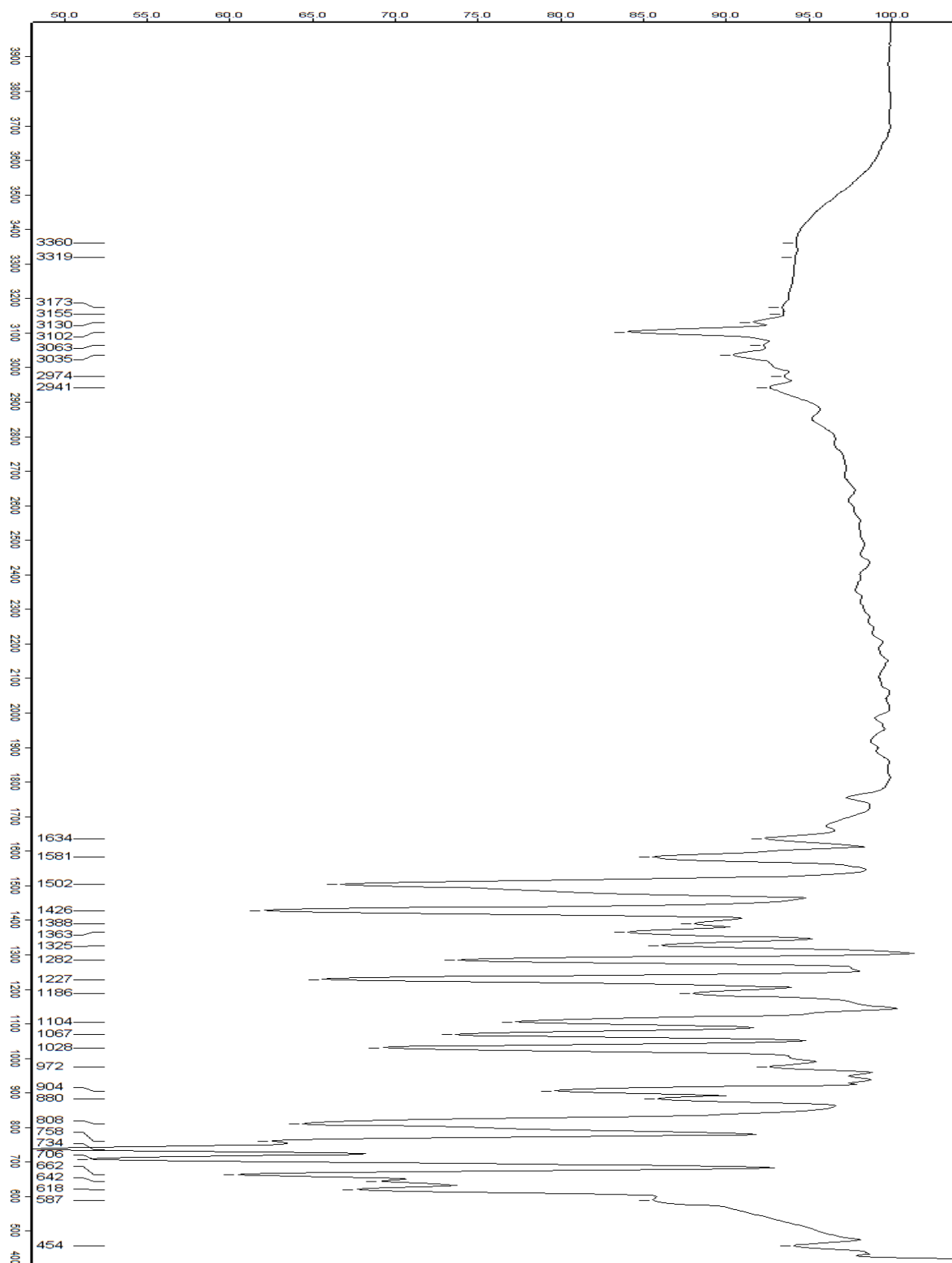
IR Spectrum of 4
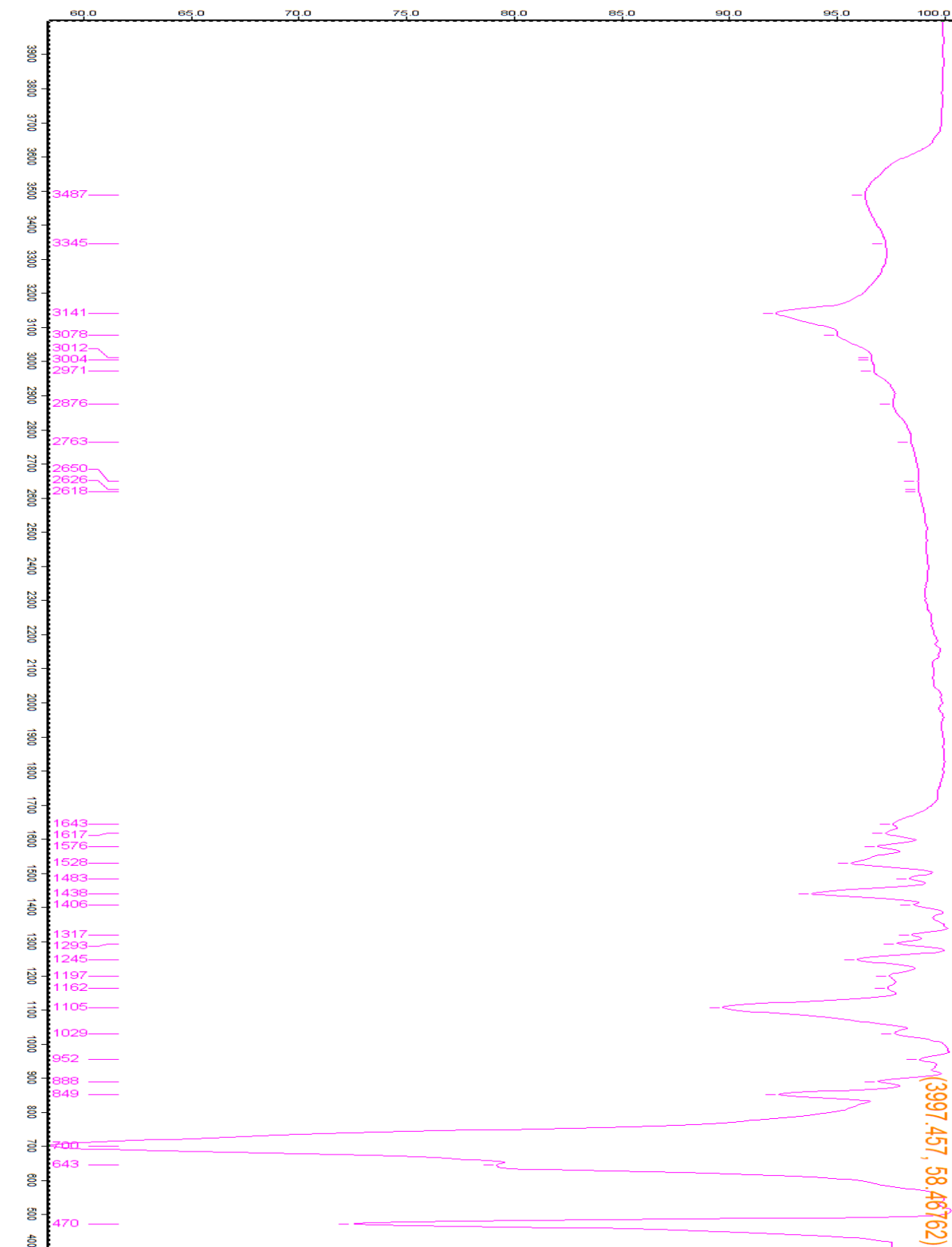
IR Spectrum of 5
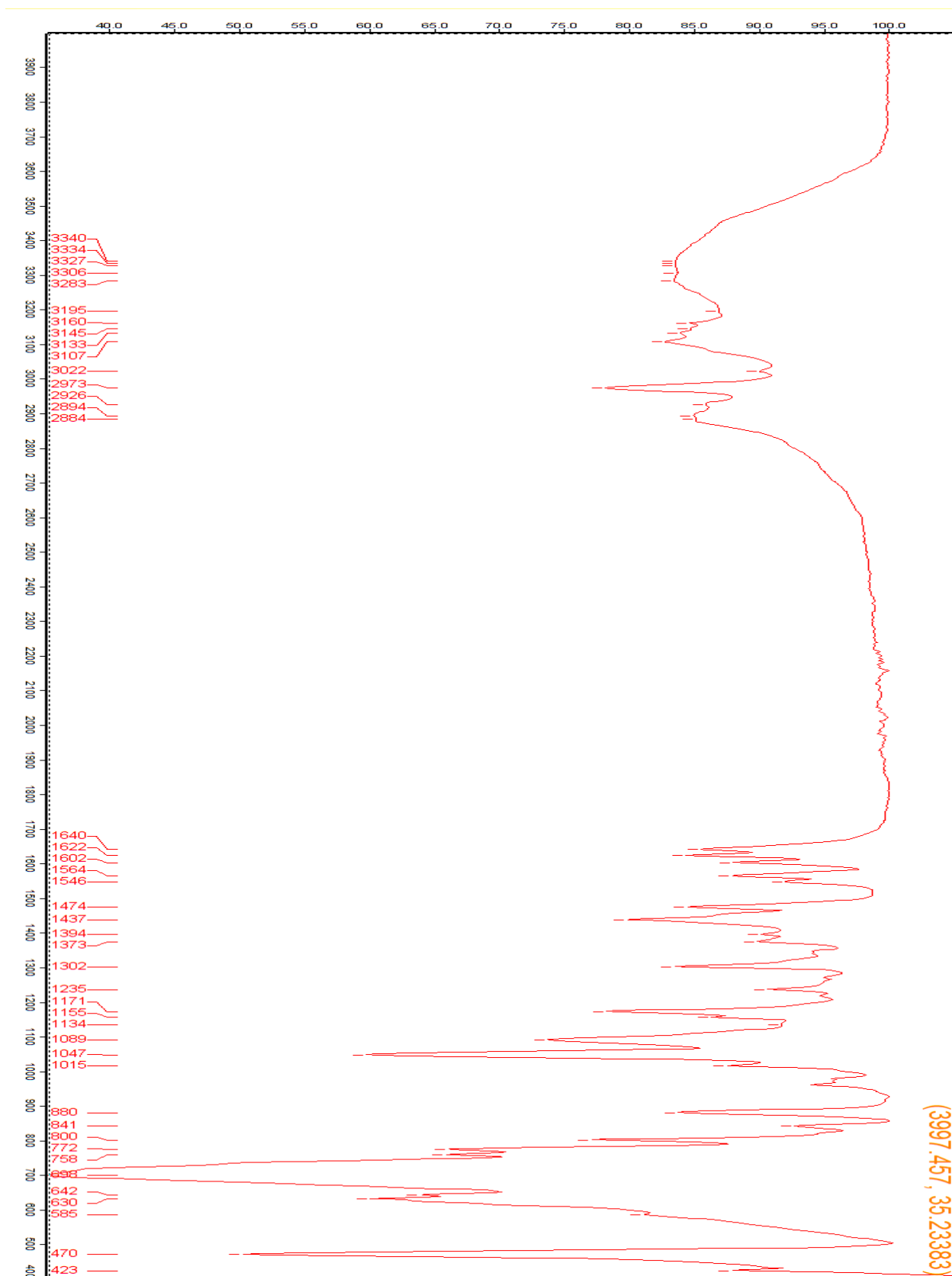
IR Spectrum of 6
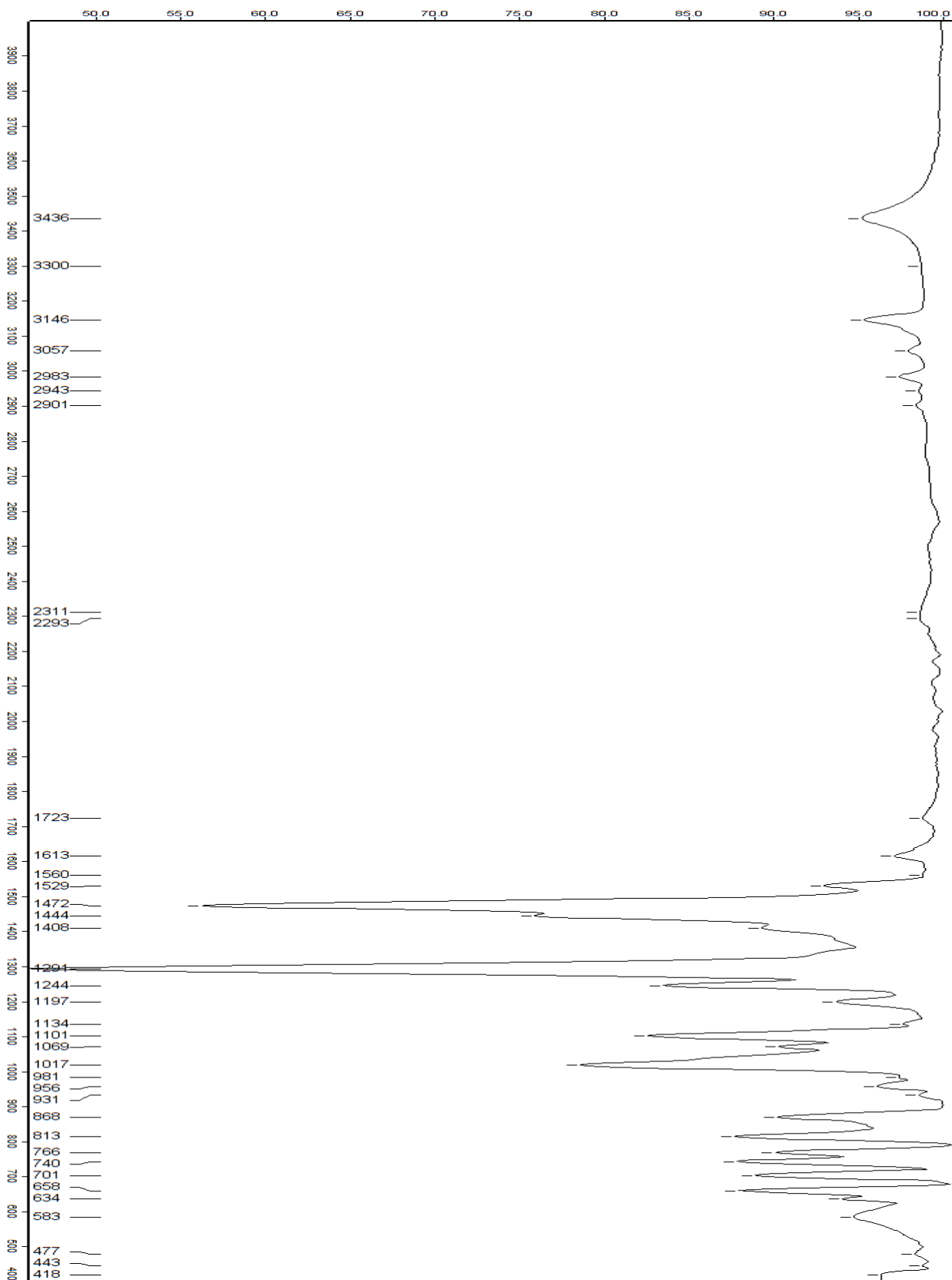
IR Spectrum of 7
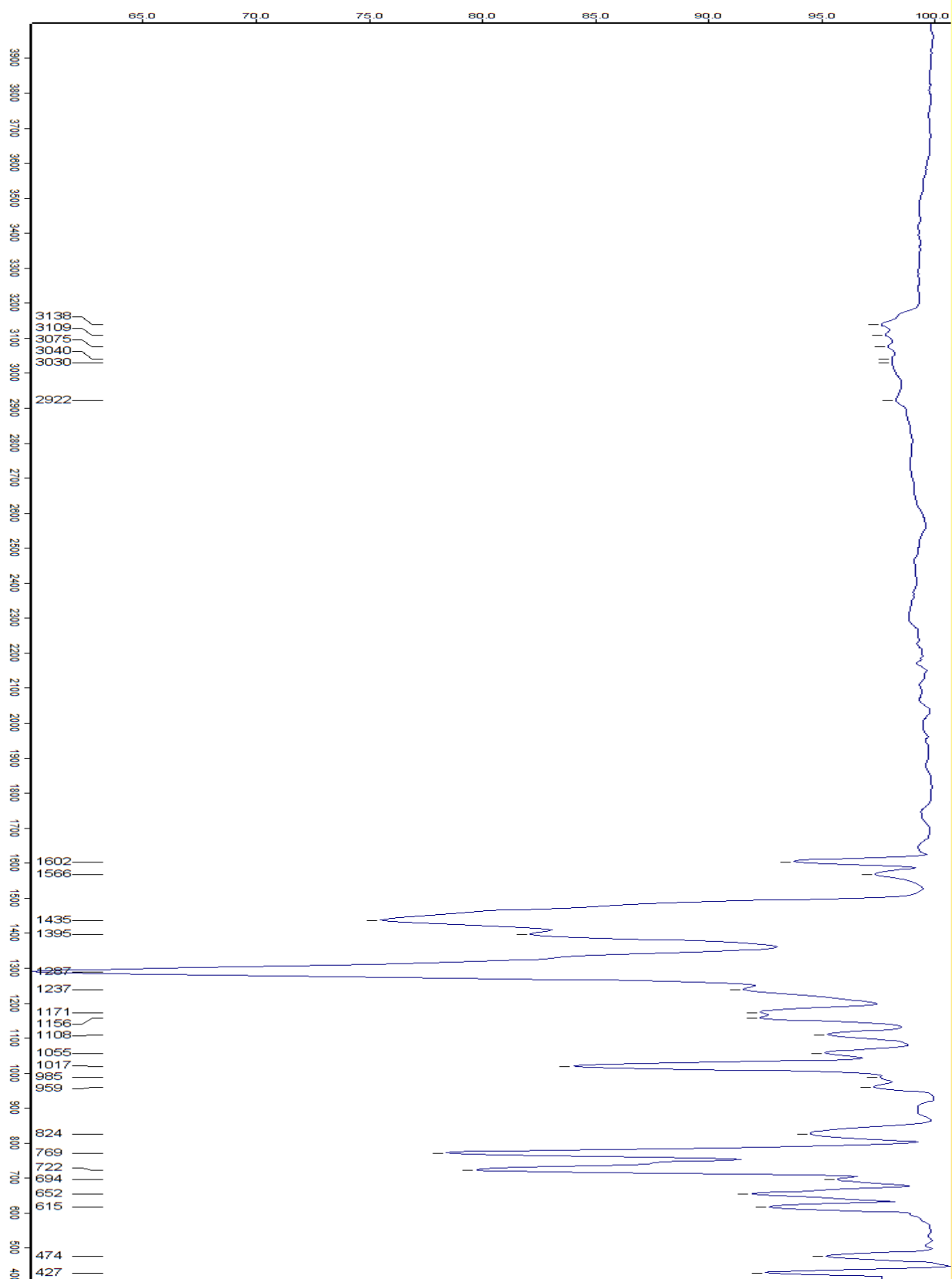
IR Spectrum of 8

7.2. Appendix B: Crystal Structure Data

Complex 1:
Table 1 Crystal data and structure refinement for do049.

Identification code	do049
Empirical formula	$C_{27}H_{27}Cu_2F_6N_3OSi$
Formula weight	678.68
Temperature/K	125.05
Crystal system	monoclinic
Space group	$P2_1/c$
a/Å	9.1395(12)
b/Å	13.9854(18)
c/Å	20.653(3)
α/°	90
β/°	90.019(2)
γ/°	90
Volume/Å^3	2639.8(6)
Z	4
ρ_{calc}g/cm^3	1.708
μ/mm^{-1}	1.727
F(000)	1376.0
Crystal size/mm^3	0.07089 × 0.03336 × 0.000472
Radiation	MoKα (λ = 0.71073)
2Θ range for data collection/°	1.972 to 58.382
Index ranges	-12 ≤ h ≤ 11, -19 ≤ k ≤ 18, -27 ≤ l ≤ 27
Reflections collected	33395
Independent reflections	6805 [R_{int} = 0.0587, R_{sigma} = 0.0535]
Data/restraints/parameters	6805/267/347
Goodness-of-fit on F^2	1.045
Final R indexes [I>=2σ (I)]	R_1 = 0.0711, wR_2 = 0.1917
Final R indexes [all data]	R_1 = 0.1044, wR_2 = 0.2150
Largest diff. peak/hole / e Å^{-3}	1.82/-0.64

Table 2 Fractional Atomic Coordinates (×10^4) and Equivalent Isotropic Displacement Parameters (Å^2×10^3) for do049. U$_{eq}$ is defined as 1/3 of of the trace of the orthogonalised U$_{IJ}$ tensor.

Atom	x	y	z	U(eq)
Cu1	5000	0	5000	19.6(2)
Cu2	10000	5000	5000	17.1(2)
Si1	8220(2)	6728.6(11)	6443.6(8)	27.1(3)
F1	9041(4)	6002(2)	5903.1(16)	30.3(8)
F2	8858(5)	6074(3)	7059.0(18)	41.5(9)
F3	9734(7)	7394(3)	6471(3)	74.2(16)

F4	6720(5)	6032(4)	6426(3)	75.0(15)
F5	7433(7)	7465(4)	6976.8(17)	62.5(13)
F6	7569(8)	7391(4)	5823(2)	84.4(19)
O1	4027(5)	967(3)	4085(2)	32.5(10)
O2	4778(13)	4914(5)	7021(4)	106(3)
O3	14741(12)	8363(7)	7040(4)	111(3)
O4	11825(12)	9602(6)	7164(4)	108(3)
O5	12174(11)	7482(7)	7209(4)	107(3)
O6	9044(12)	9500(6)	6738(3)	104(3)
N1	9202(6)	1040(3)	5187(2)	23.1(10)
N2	6988(5)	552(3)	4921(2)	19.8(9)
N3	10412(5)	3956(3)	5667(2)	20.3(10)
N4	4184(5)	−3945(3)	4895(2)	20.6(9)
N5	1962(5)	−4417(3)	5116(2)	17.8(9)
N6	5425(5)	−1090(3)	4364(2)	17.8(9)
C1	7983(6)	594(4)	5394(3)	20.5(11)
C2	8969(8)	1299(4)	4563(3)	32.0(14)
C3	7617(7)	998(4)	4396(3)	26.9(12)
C4	10501(7)	1255(4)	5590(3)	23.7(12)
C5	10473(6)	2255(4)	5866(3)	21.7(11)
C6	10447(10)	2402(5)	6522(3)	43.8(19)
C7	10438(11)	3353(5)	6746(3)	50(2)
C8	10412(9)	4103(4)	6313(3)	35.3(16)
C9	10440(6)	3044(3)	5449(3)	17.0(11)
C10	2983(6)	−4380(3)	4665(3)	18.1(11)
C11	3918(7)	−3685(4)	5526(3)	24.1(12)
C12	2539(7)	−3976(4)	5654(3)	22.8(11)
C13	5536(7)	−3768(4)	4537(3)	26.5(13)
C14	5559(6)	−2788(3)	4227(3)	18.4(11)
C15	5849(8)	−2651(4)	3584(3)	32.9(14)
C16	5982(10)	−1726(5)	3332(3)	42.5(18)
C17	5763(8)	−978(4)	3738(3)	26.7(13)
C18	5361(6)	−1975(3)	4598(3)	20.6(12)

Table 3 Anisotropic Displacement Parameters (Å^2×10^3) for do049. The Anisotropic displacement factor exponent takes the form: -2π^2[h^{2}a*^{2}U$_{11}$+2hka*b*U$_{12}$+…].

Atom	U$_{11}$	U$_{22}$	U$_{33}$	U$_{23}$	U$_{13}$	U$_{12}$
Cu1	20.0(5)	9.8(4)	29.0(5)	−1.9(3)	4.4(9)	−2.2(3)
Cu2	15.1(4)	13.0(4)	23.1(4)	1.3(3)	−0.8(8)	−3.1(3)
Si1	34.2(8)	27.1(7)	20.0(7)	−1.6(6)	4.3(7)	4.7(7)
F1	34(2)	34.4(18)	22.6(16)	−0.9(14)	6.0(16)	5.4(16)
F2	51(2)	42(2)	31.1(19)	5.4(15)	−3.0(17)	1.3(19)
F3	105(4)	59(3)	59(3)	−9(2)	28(3)	−52(3)
F4	34(2)	132(4)	59(3)	−28(3)	10(2)	−22(3)
F5	101(3)	62(2)	25.3(18)	−6(2)	18(3)	38(2)
F6	136(5)	89(3)	28(2)	7(2)	11(3)	82(3)
O1	38(3)	19.9(19)	40(2)	8.2(18)	2(2)	4(2)
O2	187(10)	67(5)	63(4)	−1(3)	−8(6)	−60(5)
O3	135(8)	142(8)	56(4)	23(5)	7(5)	34(6)
O4	166(8)	85(5)	73(5)	−40(4)	58(6)	−36(6)
O5	128(8)	106(6)	87(5)	11(5)	20(5)	−10(6)
O6	173(9)	85(5)	53(4)	8(4)	1(5)	18(6)
N1	24(2)	13(2)	32(2)	−1.8(16)	5.3(18)	−2.5(17)
N2	19(2)	12.2(18)	28(2)	−2.1(17)	7.8(19)	−2.4(16)
N3	24(3)	14.5(18)	22(2)	−2.7(16)	−4.2(18)	−0.8(18)
N4	15(2)	11.0(18)	36(2)	2.0(17)	2.2(18)	−0.1(16)
N5	16(2)	13.5(18)	24(2)	−1.4(16)	2.2(18)	−0.9(17)
N6	16(2)	9.2(17)	28(2)	−1.2(15)	2.6(18)	−1.1(16)
C1	14(2)	13(2)	34(3)	−1.9(19)	2(2)	−2.3(19)
C2	34(3)	30(3)	33(3)	3(2)	8(2)	−11(3)
C3	34(3)	18(3)	28(3)	2(2)	2(2)	−6(2)
C4	20(3)	11(2)	40(3)	−1(2)	0(2)	2.8(19)
C5	19(3)	16(2)	30(3)	−0.6(18)	0(2)	1.5(19)
C6	75(6)	31(3)	25(3)	3(2)	−2(3)	3(3)
C7	94(7)	33(3)	22(3)	−1(2)	−4(3)	6(3)
C8	57(5)	20(2)	29(3)	−6(2)	−7(3)	5(3)
C9	16(3)	15(2)	20(2)	−3.2(16)	−0.2(19)	−2.8(18)
C10	14(2)	11(2)	29(2)	1.4(18)	1.8(19)	2.9(19)
C11	25(3)	14(2)	34(3)	−5(2)	2(2)	−3(2)
C12	29(3)	14(2)	26(2)	−4.1(19)	1(2)	−4(2)
C13	16(3)	12(2)	51(3)	4(2)	9(2)	−0.2(19)
C14	12(2)	12(2)	32(3)	−2.4(18)	1(2)	1.6(18)
C15	51(4)	15(2)	33(3)	−8(2)	6(3)	−1(2)
C16	74(5)	27(3)	26(3)	−4(2)	6(3)	2(3)
C17	40(4)	17(2)	23(2)	2.1(18)	0(2)	−1(2)
C18	20(3)	12(2)	30(3)	−1.5(17)	5(2)	2.2(18)

Table 4 Bond Lengths for do049.

Atom	Atom	Length/Å	Atom	Atom	Length/Å
Cu1	N2[1]	1.981(5)	N4	C10	1.341(7)
Cu1	N2	1.981(5)	N4	C11	1.375(8)
Cu1	N6	2.050(4)	N4	C13	1.461(7)
Cu1	N6[1]	2.050(4)	N5	Cu2[4]	1.985(5)
Cu2	N3[2]	2.042(4)	N5	C10	1.319(7)
Cu2	N3	2.042(4)	N5	C12	1.375(7)
Cu2	N5[3]	1.985(5)	N6	C17	1.337(7)
Cu2	N5[1]	1.985(5)	N6	C18	1.331(6)
Si1	F1	1.685(4)	C2	C3	1.351(9)
Si1	F2	1.671(4)	C4	C5	1.510(7)
Si1	F3	1.669(5)	C5	C6	1.372(9)
Si1	F4	1.682(5)	C5	C9	1.398(7)
Si1	F5	1.671(4)	C6	C7	1.408(9)
Si1	F6	1.689(5)	C7	C8	1.379(9)
N1	C1	1.347(7)	C11	C12	1.350(8)
N1	C2	1.355(8)	C13	C14	1.514(7)
N1	C4	1.480(8)	C14	C15	1.367(9)
N2	C1	1.335(8)	C14	C18	1.382(7)
N2	C3	1.378(7)	C15	C16	1.400(8)
N3	C8	1.350(7)	C16	C17	1.356(8)
N3	C9	1.353(6)			

[1]1-X,-Y,1-Z; [2]2-X,1-Y,1-Z; [3]1+X,1+Y,+Z; [4]-1+X,-1+Y,+Z

Table 5 Bond Angles for do049.

Atom	Atom	Atom	Angle/°	Atom	Atom	Atom	Angle/°
N2[1]	Cu1	N2	180.0	C8	N3	C9	118.1(5)
N2	Cu1	N6	93.62(17)	C9	N3	Cu2	117.0(4)
N2[1]	Cu1	N6[1]	93.62(17)	C10	N4	C11	108.0(5)
N2	Cu1	N6[1]	86.38(17)	C10	N4	C13	126.2(5)
N2[1]	Cu1	N6	86.38(17)	C11	N4	C13	125.8(5)
N6[1]	Cu1	N6	180.0	C10	N5	Cu2[4]	124.7(4)
N3	Cu2	N3[2]	180.00(19)	C10	N5	C12	106.4(5)
N5[3]	Cu2	N3[2]	87.37(18)	C12	N5	Cu2[4]	128.9(4)
N5[3]	Cu2	N3	92.63(18)	C17	N6	Cu1	125.2(4)
N5[1]	Cu2	N3[2]	92.63(18)	C18	N6	Cu1	116.8(4)
N5[1]	Cu2	N3	87.37(18)	C18	N6	C17	118.0(5)

N5[1]	Cu2	N5[3]	180.00(12)	N2	C1	N1	110.6(5)
F1	Si1	F6	89.1(2)	C3	C2	N1	107.7(6)
F2	Si1	F1	91.05(19)	C2	C3	N2	108.7(6)
F2	Si1	F4	89.0(3)	N1	C4	C5	112.8(5)
F2	Si1	F6	179.8(3)	C6	C5	C4	120.7(5)
F3	Si1	F1	89.4(2)	C6	C5	C9	119.3(5)
F3	Si1	F2	89.5(3)	C9	C5	C4	119.9(5)
F3	Si1	F4	178.4(3)	C5	C6	C7	117.8(6)
F3	Si1	F5	89.5(3)	C8	C7	C6	120.3(6)
F3	Si1	F6	90.7(3)	N3	C8	C7	121.7(5)
F4	Si1	F1	90.0(2)	N3	C9	C5	122.7(5)
F4	Si1	F6	90.8(4)	N5	C10	N4	110.3(5)
F5	Si1	F1	178.8(3)	C12	C11	N4	105.8(5)
F5	Si1	F2	89.2(2)	C11	C12	N5	109.5(5)
F5	Si1	F4	91.2(3)	N4	C13	C14	112.3(5)
F5	Si1	F6	90.6(2)	C15	C14	C13	122.7(5)
C1	N1	C2	107.2(5)	C15	C14	C18	116.6(5)
C1	N1	C4	125.4(5)	C18	C14	C13	120.6(5)
C2	N1	C4	127.3(5)	C14	C15	C16	120.5(5)
C1	N2	Cu1	125.5(4)	C17	C16	C15	118.0(6)
C1	N2	C3	105.8(5)	N6	C17	C16	122.8(5)
C3	N2	Cu1	128.6(4)	N6	C18	C14	123.9(5)
C8	N3	Cu2	123.9(4)				

[1]1-X,-Y,1-Z; [2]2-X,1-Y,1-Z; [3]1+X,1+Y,+Z; [4]-1+X,-1+Y,+Z

Table 6 Torsion Angles for do049.

A	B	C	D	Angle/°	A	B	C	D	Angle/°
Cu1	N2	C1	N1	−178.0(3)	C4	C5	C9	N3	179.9(5)
Cu1	N2	C3	C2	177.5(4)	C5	C6	C7	C8	2.0(13)
Cu1	N6	C17	C16	−177.5(6)	C6	C5	C9	N3	1.3(10)
Cu1	N6	C18	C14	177.2(5)	C6	C7	C8	N3	−0.8(13)
Cu2	N3	C8	C7	168.4(6)	C8	N3	C9	C5	−0.2(9)
Cu2	N3	C9	C5	−169.4(4)	C9	N3	C8	C7	−0.1(11)
Cu2[1]	N5	C10	N4	−179.8(3)	C9	C5	C6	C7	−2.2(11)
Cu2[1]	N5	C12	C11	179.7(4)	C10	N4	C11	C12	−0.2(6)
N1	C2	C3	N2	0.6(7)	C10	N4	C13	C14	93.8(6)
N1	C4	C5	C6	118.2(7)	C10	N5	C12	C11	−0.7(6)
N1	C4	C5	C9	−60.3(7)	C11	N4	C10	N5	−0.3(6)
N4	C11	C12	N5	0.6(6)	C11	N4	C13	C14	−85.6(7)

N4	C13	C14	C15	−127.5(7)	C12 N5	C10 N4	0.6(6)
N4	C13	C14	C18	56.1(8)	C13 N4	C10 N5	−179.8(4)
C1	N1	C2	C3	−0.8(6)	C13 N4	C11 C12	179.3(5)
C1	N1	C4	C5	−95.4(6)	C13 C14	C15 C16	−174.5(7)
C1	N2	C3	C2	−0.1(6)	C13 C14	C18 N6	177.2(5)
C2	N1	C1	N2	0.7(6)	C14 C15	C16 C17	−2.2(12)
C2	N1	C4	C5	80.0(7)	C15 C14	C18 N6	0.6(9)
C3	N2	C1	N1	−0.4(6)	C15 C16	C17 N6	−0.3(12)
C4	N1	C1	N2	176.9(4)	C17 N6	C18 C14	−3.0(9)
C4	N1	C2	C3	−176.9(5)	C18 N6	C17 C16	2.8(10)
C4	C5	C6	C7	179.3(7)	C18 C14	C15 C16	2.0(10)

[1]-1+X,-1+Y,+Z

Table 7 Hydrogen Atom Coordinates ($\mathring{A}\times10^4$) and Isotropic Displacement Parameters ($\mathring{A}^2\times10^3$) for do049.

Atom	x	y	z	U(eq)
H2	9636	1633	4293	38
H3	7173	1080	3983	32
H4A	11394	1176	5324	28
H4B	10551	790	5950	28
H6	10434	1879	6816	53
H7	10451	3478	7198	59
H8	10393	4739	6473	42
H9	10438	2934	4995	20
H11	4569	−3367	5813	29
H12	2044	−3890	6054	27
H13A	5646	−4261	4196	32
H13B	6378	−3827	4836	32
H15	5962	−3187	3307	40
H16	6217	−1625	2889	51
H17	5855	−347	3572	32
H18	5168	−2054	5046	25

Experimental

Single crystals of $C_{27}H_{27}Cu_2F_6N_3OSi$ **[do049]** were **[]**. A suitable crystal was selected and **[]** on a diffractometer. The crystal was kept at 125.05 K during data collection. Using Olex2 [1], the structure was solved with the SIR2004 [2] structure solution program using Direct Methods and refined with the ShelXL [3] refinement package using Least Squares minimisation.

1. Dolomanov, O.V., Bourhis, L.J., Gildea, R.J, Howard, J.A.K. & Puschmann, H. (2009), J. Appl. Cryst. 42, 339-341.

2. Burla, M.C., Caliandro, R., Camalli, M., Carrozzini, B., Cascarano, G.L., De Caro, L., Giacovazzo, C., Polidori, G., Siliqi, D., Spagna, R. (2007). J. Appl. Cryst. 40, 609-613.
3. Sheldrick, G.M. (2015). Acta Cryst. C71, 3-8.

Crystal structure determination of [do049]

Crystal Data for $C_{27}H_{27}Cu_2F_6N_3OSi$ (M =678.68 g/mol): monoclinic, space group P2$_1$/c (no. 14), a = 9.1395(12) Å, b = 13.9854(18) Å, c = 20.653(3) Å, β = 90.019(2)°, V = 2639.8(6) Å^3, Z = 4, T = 125.05 K, μ(MoKα) = 1.727 mm^{-1}, $Dcalc$ = 1.708 g/cm^3, 33395 reflections measured (1.972° ≤ 2Θ ≤ 58.382°), 6805 unique (R_{int} = 0.0587, R$_{sigma}$ = 0.0535) which were used in all calculations. The final R_1 was 0.0711 (I > 2σ(I)) and wR_2 was 0.2150 (all data).

Refinement model description

Number of restraints - 267, number of constraints - unknown.

Details:
```
1. Twinned data refinement
 Scales: 0.556(3) 0.444(3)
2. Fixed Uiso
 At 1.2 times of:
  All C(H) groups, All C(H,H) groups
3. Rigid body (RIGU) restrains
 All non-hydrogen atoms
 with sigma for 1-2 distances of 0.004 and sigma for 1-3 distances of 0.004
4.a Secondary CH2 refined with riding coordinates:
 C4(H4A,H4B), C13(H13A,H13B)
4.b Aromatic/amide H refined with riding coordinates:
 C2(H2), C3(H3), C6(H6), C7(H7), C8(H8), C9(H9), C11(H11), C12(H12), C15(H15),
 C16(H16), C17(H17), C18(H18)
```

Complex 2:
Table 1 Crystal data and structure refinement for DO060_0ma.

Identification code	DO060_0ma
Empirical formula	$C_{17}H_{22}CuF_6N_4O_2Si$
Formula weight	520.01
Temperature/K	125.41
Crystal system	orthorhombic
Space group	Pna2$_1$
a/Å	16.2268(4)
b/Å	8.0772(2)
c/Å	15.3899(4)
α/°	90
β/°	90
γ/°	90
Volume/Å^3	2017.11(9)
Z	4
ρ_{calc}g/cm^3	1.712
μ/mm^{-1}	1.220
F(000)	1060.0
Crystal size/mm^3	0.06472 × 0.05872 × 0.02108
Radiation	MoKα (λ = 0.71073)
2Θ range for data collection/°	5.02 to 57.742

Index ranges	$-21 \leq h \leq 21, -10 \leq k \leq 10, -20 \leq l \leq 20$
Reflections collected	33882
Independent reflections	5051 [R_{int} = 0.0553, R_{sigma} = 0.0452]
Data/restraints/parameters	5051/4/286
Goodness-of-fit on F^2	1.027
Final R indexes [I>=2σ (I)]	R_1 = 0.0309, wR_2 = 0.0674
Final R indexes [all data]	R_1 = 0.0389, wR_2 = 0.0708
Largest diff. peak/hole / e Å^{-3}	0.42/-0.42
Flack parameter	0.005(6)

Table 2 Fractional Atomic Coordinates ($\times 10^4$) and Equivalent Isotropic Displacement Parameters ($Å^2 \times 10^3$) for DO060_0ma. U_{eq} is defined as 1/3 of of the trace of the orthogonalised U_{IJ} tensor.

Atom	x	y	z	U(eq)
Cu1	7060.0(2)	3236.0(5)	5050.8(3)	15.56(10)
O1	6083.5(14)	2053(3)	4569.6(16)	19.8(5)
N1	8635.5(16)	4972(3)	5273.6(17)	16.3(6)
N2	8256.5(17)	3724(4)	6429.0(18)	15.1(6)
N3	6470.2(17)	3436(3)	6229.5(19)	17.3(6)
N3'	7649.6(18)	3442(4)	3853.8(19)	17.4(6)
C1	8035.4(18)	4041(4)	5609(2)	15.0(7)
C2	9005(2)	4485(5)	6621(2)	22.0(8)
C3	9243(2)	5273(5)	5888(2)	21.7(8)
C4	7748(2)	2701(4)	7007(2)	16.6(7)
C4'	8567(2)	5679(4)	4404(2)	17.6(7)
C5	6860(2)	3294(4)	6999(2)	16.0(7)
C5'	8302.3(19)	4453(4)	3710(2)	15.6(7)
C6	5681(2)	3977(4)	6237(2)	20.7(7)
C6'	7401(2)	2484(5)	3193(2)	20.6(7)
C7	5257(2)	4303(5)	6993(2)	22.9(8)
C7'	7743(2)	2516(5)	2373(2)	23.8(8)
C8	5653(2)	4134(4)	7781(2)	20.6(7)
C8'	8412(2)	3560(5)	2228(2)	23.9(8)
C9	6474(2)	3643(4)	7778(2)	19.3(7)

C9'	8694(2)	4512(4)	2910(2)	19.7(7)
C10	5430(2)	2595(5)	4012(3)	28.7(9)
Si1	6061.3(5)	7500.8(12)	4325.9(6)	14.13(18)
F1	6592.5(11)	6268(2)	5001.1(16)	27.1(5)
F2	5548.8(12)	8808(3)	3666.8(13)	22.4(4)
F3	6169.0(12)	6147(3)	3514.0(14)	24.5(5)
F4	6963.7(11)	8450(3)	4041.4(13)	20.9(5)
F5	5979.9(11)	8958(2)	5138.5(13)	20.1(4)
F6	5171.8(11)	6654(2)	4652.1(13)	20.4(4)
O2	7609.8(14)	425(3)	5319.1(17)	24.7(6)
C11	8465(2)	85(5)	5204(3)	35.3(11)

Table 3 Anisotropic Displacement Parameters ($Å^2\times10^3$) for DO060_0ma. The Anisotropic displacement factor exponent takes the form: $-2\pi^2[h^2a^{*2}U_{11}+2hka^*b^*U_{12}+\ldots]$.

Atom	U_{11}	U_{22}	U_{33}	U_{23}	U_{13}	U_{12}
Cu1	10.92(16)	21.6(2)	14.19(17)	0.6(2)	−1.05(18)	−2.81(15)
O1	15.0(12)	19.6(13)	24.7(14)	2.6(10)	−6.2(10)	−2.3(10)
N1	12.0(12)	21.2(15)	15.9(14)	−0.4(11)	−0.9(10)	−0.8(11)
N2	11.9(13)	18.8(16)	14.7(14)	0.8(12)	0.0(11)	−1.1(12)
N3	13.5(13)	18.5(15)	19.7(15)	2.0(12)	0.4(11)	−1.4(11)
N3'	14.0(14)	20.0(16)	18.2(15)	1.8(12)	−1.1(11)	1.2(11)
C1	12.4(15)	15.3(17)	17.4(16)	0.5(14)	0.3(12)	0.9(12)
C2	13.2(16)	32(2)	20.9(17)	−2.6(16)	−3.5(13)	0.2(15)
C3	10.2(15)	31(2)	23.6(18)	−4.9(16)	−2.3(14)	−3.0(14)
C4	15.7(16)	18.5(17)	15.7(16)	1.8(14)	−0.6(13)	2.0(14)
C4'	14.2(15)	20.1(18)	18.5(16)	3.3(15)	0.5(13)	−3.6(14)
C5	14.3(16)	13.0(17)	20.6(17)	1.1(14)	0.6(13)	−2.3(13)
C5'	11.5(15)	16.3(17)	19.0(17)	3.1(14)	−2.7(13)	2.8(13)
C6	12.5(15)	25(2)	24.0(18)	3.3(16)	0.0(13)	0.1(14)
C6'	21.5(18)	19.6(18)	20.8(17)	−0.3(15)	0.4(14)	−0.9(16)
C7	12.4(16)	27(2)	30(2)	2.6(17)	1.0(14)	0.4(14)
C7'	28.2(19)	24(2)	19.0(17)	−2.8(16)	−3.6(15)	5.0(16)
C8	17.4(17)	22.5(19)	21.8(17)	−1.1(15)	6.3(14)	−1.1(14)
C8'	30(2)	26(2)	15.4(17)	3.8(15)	4.5(15)	8.2(16)
C9	19.5(17)	19.8(18)	18.5(17)	1.0(15)	0.5(14)	−1.5(14)
C9'	20.1(17)	17.5(18)	21.6(18)	4.8(15)	2.4(14)	4.3(14)

C10	18.0(18)	24(2)	44(2)	1.6(18)	−15.5(17)	0.2(16)
Si1	10.4(4)	15.6(5)	16.4(4)	1.1(4)	0.6(3)	0.4(3)
F1	19.7(9)	29.4(11)	32.1(11)	11.8(12)	−0.3(11)	7.0(8)
F2	20.5(10)	24.8(11)	21.9(10)	6.0(9)	−4.4(8)	3.4(9)
F3	22.8(10)	22.9(11)	27.9(11)	−7.5(10)	7.5(9)	−4.1(9)
F4	16.1(10)	26.0(12)	20.6(11)	−2.4(9)	4.3(8)	−5.5(8)
F5	18.9(9)	23.3(10)	18.1(10)	−3.1(9)	2.8(9)	−3.5(7)
F6	12.8(10)	24.1(11)	24.3(11)	0.2(9)	4.0(8)	−4.5(8)
O2	15.5(11)	23.3(14)	35.4(15)	−7.5(11)	−5(1)	−0.1(10)
C11	17.7(16)	38(2)	50(3)	−20(2)	−4.7(18)	4.5(16)

Table 4 Bond Lengths for DO060_0ma.

Atom	Atom	Length/Å	Atom	Atom	Length/Å
Cu1	O1	1.993(2)	C4	C5	1.518(4)
Cu1	N3	2.057(3)	C4'	C5'	1.518(5)
Cu1	N3'	2.082(3)	C5	C9	1.382(5)
Cu1	C1	1.915(3)	C5'	C9'	1.387(5)
Cu1	F1	2.5646(19)	C6	C7	1.376(5)
Cu1	O2	2.474(3)	C6'	C7'	1.380(5)
O1	C10	1.433(4)	C7	C8	1.379(5)
N1	C1	1.334(4)	C7'	C8'	1.392(6)
N1	C3	1.387(4)	C8	C9	1.391(5)
N1	C4'	1.459(4)	C8'	C9'	1.379(5)
N2	C1	1.337(4)	Si1	F1	1.678(2)
N2	C2	1.393(4)	Si1	F2	1.684(2)
N2	C4	1.468(4)	Si1	F3	1.670(2)
N3	C5	1.347(5)	Si1	F4	1.710(2)
N3	C6	1.354(4)	Si1	F5	1.723(2)
N3'	C5'	1.355(4)	Si1	F6	1.674(2)
N3'	C6'	1.340(5)	O2	C11	1.425(4)
C2	C3	1.352(5)			

Table 5 Bond Angles for DO060_0ma.

Atom	Atom	Atom	Angle/°	Atom	Atom	Atom	Angle/°
O1	Cu1	N3	89.74(11)	N2	C4	C5	110.5(3)
O1	Cu1	N3'	94.30(11)	N1	C4'	C5'	114.3(3)
O1	Cu1	F1	102.21(9)	N3	C5	C4	118.7(3)
O1	Cu1	O2	84.77(9)	N3	C5	C9	122.2(3)
N3	Cu1	N3'	170.90(11)	C9	C5	C4	119.2(3)
N3	Cu1	F1	79.27(9)	N3'	C5'	C4'	120.0(3)
N3	Cu1	O2	95.31(10)	N3'	C5'	C9'	121.6(3)
N3'	Cu1	F1	91.90(10)	C9'	C5'	C4'	118.2(3)
N3'	Cu1	O2	93.18(10)	N3	C6	C7	122.8(3)
C1	Cu1	O1	170.67(12)	N3'	C6'	C7'	124.3(4)
C1	Cu1	N3	87.85(12)	C6	C7	C8	119.4(3)
C1	Cu1	N3'	89.41(12)	C6'	C7'	C8'	118.1(4)
C1	Cu1	F1	86.19(11)	C7	C8	C9	118.2(3)
C1	Cu1	O2	86.48(12)	C9'	C8'	C7'	118.4(3)
O2	Cu1	F1	171.04(8)	C5	C9	C8	119.7(3)
C10	O1	Cu1	131.7(2)	C8'	C9'	C5'	120.3(3)
C1	N1	C3	110.7(3)	F1	Si1	F2	177.58(13)
C1	N1	C4'	121.3(3)	F1	Si1	F4	89.14(11)
C3	N1	C4'	127.6(3)	F1	Si1	F5	89.74(12)
C1	N2	C2	110.5(3)	F2	Si1	F4	89.28(11)
C1	N2	C4	121.9(3)	F2	Si1	F5	88.33(11)

C2	N2	C4	127.6(3)	F3	Si1	F1	91.19(12)
C5	N3	Cu1	123.3(2)	F3	Si1	F2	90.67(11)
C5	N3	C6	117.7(3)	F3	Si1	F4	90.72(10)
C6	N3	Cu1	118.3(2)	F3	Si1	F5	177.38(12)
C5'	N3'	Cu1	123.5(2)	F3	Si1	F6	92.69(11)
C6'	N3'	Cu1	119.1(2)	F4	Si1	F5	86.85(10)
C6'	N3'	C5'	117.3(3)	F6	Si1	F1	90.83(11)
N1	C1	Cu1	128.4(2)	F6	Si1	F2	90.64(11)
N1	C1	N2	106.1(3)	F6	Si1	F4	176.59(12)
N2	C1	Cu1	125.5(2)	F6	Si1	F5	89.74(10)
C3	C2	N2	106.3(3)	Si1	F1	Cu1	137.50(13)
C2	C3	N1	106.4(3)	C11	O2	Cu1	120.5(2)

Table 6 Hydrogen Bonds for DO060_0ma.

D	H	A	d(D-H)/Å	d(H-A)/Å	d(D-A)/Å	D-H-A/°
O1	H1	F5[1]	0.867(12)	1.797(14)	2.654(3)	169(3)
O2	H2A	F4[1]	0.84	1.93	2.741(3)	161.9

[1]+X,-1+Y,+Z

Table 7 Hydrogen Atom Coordinates (Å×10^4) and Isotropic Displacement Parameters (Å^2×10^3) for DO060_0ma.

Atom	x	y	z	U(eq)
H1	5982(17)	1070(20)	4760(20)	30
H2	9291	4456	7159	26
H3	9731	5907	5809	26
H4A	7968	2760	7606	20
H4B	7771	1532	6815	20
H4'A	9108	6150	4238	21
H4'B	8165	6599	4420	21
H6	5407	4138	5698	25
H6'	6961	1734	3297	25
H7	4696	4641	6972	28
H7'	7529	1844	1919	29
H8	5372	4348	8311	25

H8'	8667	3616	1673	29
H9	6768	3548	8309	23
H9'	9159	5210	2831	24
H10A	5420	1908	3487	43
H10B	5521	3754	3849	43
H10C	4903	2494	4318	43
H2A	7331	−221	5009	37
H11A	8608	198	4588	53
H11B	8583	−1047	5397	53
H11C	8791	869	5547	53

Plane 1	Plane 2	Fold Angle/°	Twist Angle/°
C1, C2, C3, N1, N2	C5, C6, C7, C8, C9, N3	51.5372(14)	3.3229(14)
C1, C2, C3, N1, N2	C5', C6', C7', C8', C9', N3	35.0629(10)	0.3414(6)
C5, C6, C7, C8, C9, N3	C5', C6', C7', C8', C9', N3	14.6216(5)	57.2729(15)

Experimental

Single crystals of $C_{17}H_{22}CuF_6N_4O_2Si$ **[DO060_0ma]** were **[]**. A suitable crystal was selected and **[]** on a **'Bruker APEX-II CCD'** diffractometer. The crystal was kept at 125.41 K during data collection. Using Olex2 [1], the structure was solved with the ShelXT [2] structure solution program using Intrinsic Phasing and refined with the ShelXL [3] refinement package using Least Squares minimisation.

1. Dolomanov, O.V., Bourhis, L.J., Gildea, R.J, Howard, J.A.K. & Puschmann, H. (2009), J. Appl. Cryst. 42, 339-341.
2. Sheldrick, G.M. (2015). Acta Cryst. A71, 3-8.
3. Sheldrick, G.M. (2015). Acta Cryst. C71, 3-8.

Crystal structure determination of [DO060_0ma]

Crystal Data for $C_{17}H_{22}CuF_6N_4O_2Si$ (M =520.01 g/mol): orthorhombic, space group Pna2$_1$ (no. 33), a = 16.2268(4) Å, b = 8.0772(2) Å, c = 15.3899(4) Å, V = 2017.11(9) Å^3, Z = 4, T = 125.41 K, µ(MoKα) = 1.220 mm^{-1}, $Dcalc$ = 1.712 g/cm^3, 33882 reflections measured (5.02° ≤ 2Θ ≤ 57.742°), 5051 unique (R_{int} = 0.0553, R$_{sigma}$ = 0.0452) which were used in all calculations. The final R_1 was 0.0309 (I > 2σ(I)) and wR_2 was 0.0708 (all data).

Refinement model description

Number of restraints - 4, number of constraints - unknown.

```
Details:
1. Fixed Uiso
 At 1.2 times of:
  All C(H) groups, All C(H,H) groups
 At 1.5 times of:
  All C(H,H,H) groups, All O(H) groups
2. Restrained distances
 O1-H1
 0.87 with sigma of 0.01
 C10-H1
 1.912233 with sigma of 0.02
 Cu1-H1
 2.544082 with sigma of 0.02
```

3.a Secondary CH2 refined with riding coordinates:
 C4(H4A,H4B), C4'(H4'A,H4'B)
3.b Aromatic/amide H refined with riding coordinates:
 C2(H2), C3(H3), C6(H6), C6'(H6'), C7(H7), C7'(H7'), C8(H8), C8'(H8'), C9(H9),
 C9'(H9')
3.c Idealised Me refined as rotating group:
 C10(H10A,H10B,H10C), C11(H11A,H11B,H11C)
3.d Idealised tetrahedral OH refined as rotating group:
 O2(H2A)